BornAgain Physics Reference

Work in progress

Version 21.0

Last updated August 4, 2023

edited by Joachim Wuttke

Scientific Computing Group
Jülich Centre for Neutron Science
at Heinz Maier-Leibnitz Zentrum Garching
Forschungszentrum Jülich GmbH

For information about BornAgain, see the reference paper Pospelov et al 2020 [1] and the web docs at `https://www.bornagainproject.org`.

This reference provides some of the theory behind the code.

Notation: Bold symbols ($\mathbf{r}$, $\mathbf{B}$) are real or complex 3-vectors. A hat accent ($\hat{n}$, $\hat{\mathbf{B}}$) denotes a unit vector in three-dimensional Euklidean space. A breve accent ($\breve{v}$, $\breve{\sigma}_z$) denotes an operator in spin space, represented by a complex 2×2 matrix. Spinors are represented by uppercase letters (Ψ, Φ, T, R), but not every uppercase letter stands for a spinor. Black-board bold ($\mathbb{M}$) denotes 4×4 matrices.

Layers are numbered from 0 to $N - 1$ against the z direction, as explained in Fig. 2.2.

This is work in progress. Sections replaced by … are not yet ready for publication. Contact us to discuss them privately.

Editor: Joachim Wuttke

Authors: BornAgain developers, see AUTHORS file and git log
Scientific Computing Group
at Heinz Maier-Leibnitz Zentrum (MLZ) Garching

Contents

1 Wave propagation and scattering

This chapter introduces the formalism to described neutron and X-ray propagation and scattering, as needed for the analysis of grazing-incidence small-angle scattering (GISAS) experiments.

1.1 Wave propagation

In this section, we review the wave equations that describe the propagation of neutrons (Sec. 1.1.1) and X-rays (Sec. 1.1.2) in matter, and combine them into a unified wave equation (Sec. 1.1.3) that is the base for the all following analysis. This provides justification and background for Eqns. 1–3 in the BornAgain reference paper [1].

1.1.1 Neutrons

The scalar wavefunction $\psi(\mathbf{r},t)$ of a free neutron in absence of a magnetic field is governed by the Schrödinger equation

$$i\hbar\partial_t\psi(\mathbf{r},t) = \left\{-\frac{\hbar^2}{2m}\nabla^2 + V(\mathbf{r})\right\}\psi(\mathbf{r},t). \tag{1.1}$$

Since BornAgain only aims at modelling elastic scattering, any time dependence of the potential is averaged out in the definition $V(\mathbf{r}) := \langle V(\mathbf{r},t)\rangle$. Inelastic scattering has for only effect an attenuation along beam trajectories.[1] Therefore we only need to consider monochromatic waves with given frequency ω. In consequence, the wavefunction

$$\psi(\mathbf{r},t) = \psi(\mathbf{r})\mathrm{e}^{-i\omega t} \tag{1.2}$$

factorizes into a stationary wave and a time-dependent phase factor. In the following, we will characterize the incoming radiation not by its energy $\hbar\omega$, but by its *vacuum wavenumber* K, given by the dispersion relation

$$\hbar\omega = \frac{(\hbar K)^2}{2m}. \tag{1.3}$$

The Schrödinger equation (1.1) then takes the simple form

$$\left\{\nabla^2 + K^2 - 4\pi v_{\text{nucl}}(\mathbf{r})\right\}\psi(\mathbf{r}) = 0 \tag{1.4}$$

[1]This is not explicitly supported in the software, but users are free to increase the imaginary part of the refractive index to model inelastic and other losses.

with the rescaled form of Fermi's pseudopotential

$$v_{\text{nucl}}(\mathbf{r}) := \frac{m}{2\pi\hbar^2}V(\mathbf{r}) = \sum_j \langle b_j\delta\left(\mathbf{r}-\mathbf{r}_j(t)\right)\rangle\,. \tag{1.5}$$

The sum runs over all nuclei exposed to ψ. The subscript "nucl" designates nuclear as opposed to magnetic scattering. The *bound scattering length* b_j is isotope specific; values are tabulated [2].

In *small-angle scattering*, as elsewhere in *neutron optics* [3], the potential can be coarse-grained by spatially averaging over at least a few atomic diameters,

$$v_{\text{nucl}}(\mathbf{r}) = \sum_s b_s\rho_s(\mathbf{r}), \tag{1.6}$$

where the sum now runs over chemical elements, $b_s := \langle b_j\rangle_{j\in s}$ is the bound *coherent* scattering length, and ρ_s is a number density. In passing from (1.5) to (1.6), we neglected *Bragg scattering* from atomic-scale correlation, and *incoherent scattering* from spin or isotope related fluctuations of b_j. In small-angle experiments, these types of scattering only matter as loss channels.[2] Furthermore, incoherent scattering, as inelastic scattering, contributes to the diffuse background in the detector. In conclusion, the coarse-grained neutron optical potential (1.6) is just a *scattering length density* (SLD) [3, eq. 2.8.37], and the effective macroscopic Schrödinger equation still has the form (1.1) or (1.4).

The current density, or *flux*, of a neutron beam is given by

$$\mathbf{J}(\mathbf{r}) = \psi^*\frac{\nabla}{2i}\psi - \psi\frac{\nabla}{2i}\psi^*. \tag{1.7}$$

For a monochromatic *plane wave*

$$\psi_{\mathbf{k}}(\mathbf{r}) := \mathrm{e}^{i\mathbf{kr}} \tag{1.8}$$

note that the conjugate wave function $\psi_{\mathbf{k}}(\mathbf{r})^* = \mathrm{e}^{i\mathbf{k}^*\mathbf{r}}$ involves the conjugate of the complex wavevector $\mathbf{k}$. Accordingly, the flux is

$$\mathbf{J}(\mathbf{r}) = |\psi_{\mathbf{k}}(\mathbf{r})|^2\,\mathrm{Re}\,\mathbf{k}. \tag{1.9}$$

1.1.2 X-rays

The propagation of X-rays is governed by Maxwell's equations,

$$\begin{aligned}\nabla\times\mathbf{E} &= -\partial_t\mathbf{B}, \quad \nabla\mathbf{B}=0, \quad \mathbf{B}=\mu(\mathbf{r})\mu_0\mathbf{H},\\ \nabla\times\mathbf{H} &= +\partial_t\mathbf{D}, \quad \nabla\mathbf{D}=0, \quad \mathbf{D}=\epsilon(\mathbf{r})\epsilon_0\mathbf{E}.\end{aligned} \tag{1.10}$$

Since BornAgain only addresses elastic scattering, we assume the permeability and permittivity tensors μ and ϵ to be time-independent. Therefore, as in Sec. 1.1.1, we

[2] Same remark as in Footnote 1: To model these losses, use the imaginary part of the refractive index.

only need to consider monochromatic waves with given frequency ω, and each of the fields $\mathbf{E}$, $\mathbf{D}$, $\mathbf{H}$, $\mathbf{B}$ factorizes into a stationary field and a time-dependent phase factor.[3] We will formulate the following in terms of the electric field

$$\mathbf{E}(\mathbf{r}, t) = \mathbf{E}(\mathbf{r})\mathrm{e}^{-i\omega t}. \tag{1.11}$$

The other three fields can be obtained from $\mathbf{E}$ by straightforward application of (1.10).

Since magnetic refraction or scattering is beyong the scope of BornAgain, the relative magnetic permeability tensor is always $\mu(\mathbf{r}) = 1$. As customary in SAXS and GISAXS, we assume that the dielectric properties of the material are those of a polarizable electron cloud.[4] Thereby the relative dielectric permittivity tensor ϵ becomes a scalar,

$$\epsilon(\mathbf{r}) = 1 - \frac{4\pi r_e}{K^2}\rho(\mathbf{r}), \tag{1.12}$$

with the classical electron radius $r_e = e^2/mc^2 \simeq 2.8 \cdot 10^{-15}$ m, the electron number density $\rho(\mathbf{r})$, and the vacuum wavenumber K, given by the dispersion relation

$$K^2 = \mu_0\epsilon_0\omega^2. \tag{1.13}$$

With these simplifying assumptions about ϵ and μ, Maxwell's equations yield the wave equation

$$\nabla \times \nabla \times \mathbf{E} = K^2\epsilon(\mathbf{r})\mathbf{E}. \tag{1.14}$$

Using a standard identity from vector analysis, it can be brought into the more tractable form

$$\left\{\nabla^2 - \nabla \cdot \nabla + K^2\epsilon(\mathbf{r})\right\} \mathbf{E}(\mathbf{r}) = 0. \tag{1.15}$$

It is well known that the electromagnetic energy flux is given by the Poynting vector. However, its standard definition, $\mathbf{S} \coloneqq \mathbf{E} \times \mathbf{H}$, is not applicable here because it only holds for *real* fields. With our complex notation, it must be replaced by

$$\mathbf{S} \coloneqq \operatorname{Re}\mathbf{E}(\mathbf{r}, t) \times \operatorname{Re}\mathbf{H}(\mathbf{r}, t). \tag{1.16}$$

For stationary oscillations (1.11), the time average is

$$\langle \mathbf{S} \rangle = \frac{1}{4} \langle \mathbf{E}(\mathbf{r}) \times \mathbf{H}(\mathbf{r})^* + \text{c. c.} \rangle \, . \tag{1.17}$$

[3] This phase factor can be defined with a plus or a minus sign in the exponent. Most texts on X-ray crystallography, including influential texts on GISAXS [4], prefer the *crystallographic convention* with a plus sign. In BornAgain, we prefer the opposite *quantum-mechanical convention* for consistency with the neutron case (1.2), where the minus sign is an inevitable consequence of the standard form of the Schrödinger equation.

[4] This is occasionally called the *Laue model* [5].

We specialize to vacuum with $\epsilon(\mathbf{r}) = 1$, and obtain

$$\langle \mathbf{S} \rangle = \frac{1}{4i\omega\mu_0} \left(\mathbf{E}^*(\mathbf{r}) \times (\nabla \times \mathbf{E}(\mathbf{r})) + \text{c. c.} \right). \tag{1.18}$$

For a monochromatic plane wave $\mathbf{E}(\mathbf{r}) = \mathbf{E_k} \mathrm{e}^{i\mathbf{kr}}$, we find

$$\langle \mathbf{S} \rangle = \frac{1}{2\omega\mu_0} |\mathbf{E_k}|^2 \operatorname{Re} \mathbf{k}, \tag{1.19}$$

which confirms the common knowledge that the radiation intensity counted in a detector is proportional to the squared electric field amplitude.

1.1.3 Unified wave equation

As in Eqns. 1–3 of Ref. [1], we combine all the above in a unified wave equation

$$\left(D_0 - 4\pi v(\mathbf{r}) \right) \psi(\mathbf{r}) = 0 \tag{1.20}$$

with the vacuum wave operator

$$D_0 := \begin{cases} \nabla^2 + K^2 & \text{for neutrons,} \\ \nabla^2 - \nabla \cdot \nabla + K^2 & \text{for X-rays} \end{cases} \tag{1.21}$$

and the potential[5]

$$v(\mathbf{r}) := \begin{cases} v_{\text{nucl}}(\mathbf{r}) & \text{for neutrons,} \\ K^2(1 - \epsilon(\mathbf{r}))/(4\pi) & \text{for X-rays.} \end{cases} \tag{1.22}$$

The generic wave amplitude ψ shall represent the scalar neutron wavefunction ψ or the electric field $\mathbf{E}$.

1.2 Distorted-wave Born approximation

Neutron or X-ray scattering by condensed matter is usually described in *Born approximation* (BA), which is treats the whole potential $v(\mathbf{r})$ as a small perturbation. This is not adequate if incident or scattered wave propagate under small glancing angles, as refraction and reflection are no longer small. For grazing-incidence small-angle scattering, we need the more generic *distorted-wave Born approximation* (DWBA).[6]

[5]This corrects Eq. 3 in our reference paper [1], which had a sign error in the X-ray case.

[6]The DWBA was originally devised by Massey and Mott (ca 1933) for collisions of charged particles. Summaries can be found in some quantum mechanics textbooks (Messiah, Schiff) and in monographs on scattering theory (e. g. Newton). The first explicit applications to grazing-incidence scattering were published in 1982: Vineyard [6] discussed X-ray scattering, but failed to account for the distortion of the scattered wave; Mazur and Mills [7] deployed heavy formalism to compute the inelastic neutron scattering cross section of ferromagnetic surface spin waves from scratch. A concise derivation of the DWBA cross section was provided by Dietrich and Wagner (1984/85) for X-rays [8] and neutrons [9]. Unfortunately, their work was overlooked in much of the later literature, which often fell back to less convincing derivations.

1.2.1 Distortion versus perturbation

To get started, we decompose the potential (1.22) into a more *regular* and a more *fluctuating* part:

$$v(\mathbf{r}) =: \overline{v}(\mathbf{r}) + \delta v(\mathbf{r}). \tag{1.23}$$

The *distortion field* $\overline{v}$ comprises regular, well-known features of the sample. The *perturbation potential* δv stands for the more irregular, unknown features of the sample one ultimately wants to study in a scattering experiment. The wave equation (1.20) shall henceforth be written as

$$\left(D(\mathbf{r}) - 4\pi\delta v(\mathbf{r})\right)\psi(\mathbf{r}) = 0 \tag{1.24}$$

with the *distorted wave operator*

$$D(\mathbf{r}) := D_0 - 4\pi\overline{v}(\mathbf{r}). \tag{1.25}$$

Only δv shall be treated as a perturbation. The propagation of incident and scattered waves under the influence of $\overline{v}$, in contrast, shall be handled exactly, through analytical solution of the *unperturbed distorted wave equation*

$$D(\mathbf{r})\psi(\mathbf{r}) = 0. \tag{1.26}$$

The solutions are called *distorted* because they differ from the plane waves obtained in the vacuum case $\overline{v} = 0$.

Except for neutrons in a magnetic field the distortion field is scalar so that it can be expressed through the *refractive index*

$$n(\mathbf{r}) := \sqrt{1 - \frac{4\pi\overline{v}(\mathbf{r})}{K^2}} = \begin{cases} \sqrt{1 - 4\pi\overline{v}_{\text{nucl}}(\mathbf{r})/K^2} & \text{for neutrons,} \\ \sqrt{\epsilon(\mathbf{r})} & \text{for X-rays.} \end{cases} \tag{1.27}$$

If $\overline{v}(\mathbf{r})$ or $\epsilon(\mathbf{r})$ has an imaginary part, describing absorption, then $n(\mathbf{r})$ is a complex number. Conventionally, n is parameterized by two real numbers:

$$n =: 1 - \delta + i\beta. \tag{1.28}$$

For thermal neutrons and X-rays, δ and β are almost always nonnegative,[7] and much smaller than 1. This explains why in most scattering geometries the ordinary Born approximation with $\overline{v} \equiv 0$ is perfectly adequate. In layered samples under grazing incidence, however, even small differences in n can cause substantial *refraction* and *reflection*. To model GISAS, therefore, it is necessary to use DWBA with $\overline{v}(z)$ given by the horizontally averaged refractive index $\overline{n}(z)$.

[7] The plus sign in front of $i\beta$ is a consequence of the quantum-mechanical sign convention; in the X-ray crystallography convention it would be a minus sign.

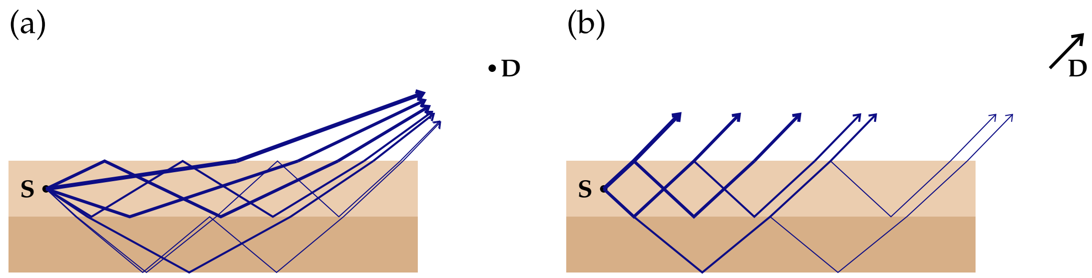

Figure 1.1: (a) In a multilayer sample, the scattered wave propagates from the scattering center S towards the detector D through different paths, due to partial reflection by interfaces. (b) In far-field approximation, the detector location is so remote that all rays leaving the sample can be considered parallel. In consequence, when the scattered wave is traced back from the detector it can be considered plane until it reaches the sample.

1.2.2 Differential cross section

The ratio of the scattered flux $J(\mathbf{r})$ hitting an infinitesimal detector area $r^2\mathrm{d}\Omega$ to the incident flux J_i is expressed as a *differential cross section*

$$\frac{\mathrm{d}\sigma}{\mathrm{d}\Omega} := \frac{r^2 J(\mathbf{r})}{J_\mathrm{i}}. \tag{1.29}$$

The geometric factors that are needed to convert $\mathrm{d}\sigma/\mathrm{d}\Omega$ into detector counts will be discussed below in Sec. 6.1.

From standard textbooks we take the generic differential cross section of elastic scattering in first order Born approximation,[8]

$$\frac{\mathrm{d}\sigma}{\mathrm{d}\Omega} = |\langle\psi_\mathrm{i}|\delta v|\psi_\mathrm{f}\rangle|^2, \tag{1.30}$$

where the matrix element in Dirac bra-ket notation stands for the integral

$$\langle\psi_\mathrm{i}|\delta v|\psi_\mathrm{f}\rangle := \int \mathrm{d}^3r\, \psi_\mathrm{i}^*(\mathbf{r})\delta v(\mathbf{r})\psi_\mathrm{f}(\mathbf{r}). \tag{1.31}$$

For brevity and mathematical convenience, the integral has no bounds and therefore formally runs over the entire space. However, $\delta v(\mathbf{r})$ is nonzero only if $\mathbf{r}$ lies inside the finite sample volume.

In ordinary (non-distorted) Born approximation, the incident ψ_i is a plane wave (1.8). By means of a far-field expansion, the outgoing spherical wave ψ_f, traced back from the detector towards the sample, is also approximated as a plane wave. Thereby (1.31) becomes a Fourier integral

$$\langle\psi_\mathrm{i}|\delta v|\psi_\mathrm{f}\rangle = \int \mathrm{d}^3r\, \mathrm{e}^{-i\mathbf{k}_\mathrm{i}\mathbf{r}}\delta v(\mathbf{r})\mathrm{e}^{i\mathbf{k}_\mathrm{f}\mathbf{r}} = \int \mathrm{d}^3r\, \mathrm{e}^{i\mathbf{q}\mathbf{r}}\delta v(\mathbf{r}) \tag{1.32}$$

with the scattering vector

$$\mathbf{q} := \mathbf{k}_\mathrm{f} - \mathbf{k}_\mathrm{i}. \tag{1.33}$$

[8] For a particularly detailed derivation see Schober's lecture notes on neutron scattering [10].

This plane-wave approximation breaks down under grazing incidence as refraction and reflection by surfaces and interfaces cannot be neglected. While (1.30) and (1.31) still hold, (1.32) does not. In DWBA, the incident wave ψ_{i} ceases to be plane when it reaches the sample (Fig. 1.1). Inside the sample it evolves according to the unperturbed wave equation (1.26). Similarly, the scattered wave ψ_{f}, traced back from the detector, is a plane wave outside the sample, but is distorted inside the sample as it obeys (1.26). The wave propagation inside a discrete multilayer sample will be worked out in Chapter 2.

2 Flat multilayer systems

This chapter specializes the DWBA for a multilayer system with $\overline{v}(\mathbf{r}) = \overline{v}(z)$.

2.1 Wave propagation and scattering in layered samples

2.1.1 Wave propagation in 2+1 dimensions

We now specialize the results from Chapter 1 to wave propagation in a sample that is, on average, translationally invariant in 2 dimensions. Following standard convention, we choose the surface of the sample in the xy plane, and its normal along z. In visualizations, we will always represent the xy plane as *horizontal*, and the z axis as upward *vertical*, altough there are "horizontal" reflectometers where the sample is upright to allow for a horizontal scattering plane.

Scattering from such systems will be studied in distorted-wave Born approximation. To determine the neutron scattering cross section (1.30), we need to determine the incident and final wavefunctions ψ_i and ψ_f. Vertical variations of the refractive index $n(z)$ cause refraction and reflection. For waves propagating at small glancing angles, the reflectance can take any value between 0 and 1, even though $1 - n$ is only of the order 10^{-5} or smaller. Such zeroth-order effects cannot be accounted for by perturbative scattering theory. Instead, we need to deal with refraction and reflection from the onset, in the wave propagation equation. Accordingly, the SLD decomposition (1.23) takes the form

$$v(\mathbf{r}) = \overline{v}(z) + \delta v(\mathbf{r}), \tag{2.1}$$

and the unperturbed distorted wave equation (1.26) becomes

$$\left\{\nabla^2 + k(z)^2\right\}\psi(\mathbf{r}) = 0. \tag{2.2}$$

Below and above the sample, $k(z) = \text{const}$: in these regions, $\psi(\mathbf{r})$ is a superposition of plane waves. The exciting wavefunction is

$$\psi_\mathrm{e}(\mathbf{r}) = \mathrm{e}^{i\mathbf{k}_\parallel \mathbf{r}_\parallel + ik_{\perp\mathrm{e}} z}, \tag{2.3}$$

The subscripts $\parallel$ and $\perp$ refer to the sample xy plane. The wavevector components $\mathbf{k}_\parallel$ and $k_\perp$ must fulfill

$$k(z)^2 = \mathbf{k}_\parallel^2 + k_\perp^2. \tag{2.4}$$

Continuity across the sample implies

$$\mathbf{k}_\parallel = \text{const.} \tag{2.5}$$

From here on, we abbreviate

$$\kappa := k_\perp. \tag{2.6}$$

When the incident wave hits the sample, it is wholly or partly reflected. Therefore, the full the solution of (2.2) in the half space of the radiation source is

$$\psi(\mathbf{r}) = \mathrm{e}^{i\mathbf{k}_\parallel\mathbf{r}_\parallel + i\kappa_\mathrm{e}z} + R\,\mathrm{e}^{i\mathbf{k}_\parallel\mathbf{r}_\parallel - i\kappa_\mathrm{e}z} \tag{2.7}$$

with a complex reflection coefficient R. The reflected flux is given by the reflectance $|R|^2$. In the opposite halfspace, the solution of (2.2) is simply

$$\psi(\mathbf{r}) = T\,\mathrm{e}^{i\mathbf{k}_\parallel\mathbf{r}_\parallel + i\kappa_\mathrm{e}z} \tag{2.8}$$

with a complex transmission coefficient T. The transmitted flux is given by the transmittance $|T|^2$. As before, subscript e stands for the exciting wave in vacuum outside the sample.

Within the sample, the wave equation (2.2) is solved by the factorization ansatz

$$\psi(\mathbf{r}) = \mathrm{e}^{i\mathbf{k}_\parallel\mathbf{r}_\parallel}\phi(z). \tag{2.9}$$

The vertical wavefunction $\phi(z)$ is governed by the one-dimensional wave equation

$$\left\{\partial_z^2 + k(z)^2 - k_\parallel^2\right\}\phi(z) = 0. \tag{2.10}$$

As solution of a differential equation of second degree, $\phi(z)$ can be written as superposition of a downward travelling wave $\phi^-(z)$ and an upward travelling wave $\phi^+(z)$. Accordingly, the three-dimensional wavefunction can be written as

$$\psi(\mathbf{r}) = \psi^-(\mathbf{r}) + \psi^+(\mathbf{r}). \tag{2.11}$$

2.1.2 The four DWBA terms

All the above holds not only for the incident wavefunction ψ_i, but also for the wavefunction ψ_f that is tracked back from a detector pixel towards the sample. Therefore the scattering matrix element involves two incident and two final partial wavefunctions. The resulting sum

$$\langle\psi_\mathrm{i}|\delta v|\psi_\mathrm{f}\rangle = \langle\psi_\mathrm{i}^-|\delta v|\psi_\mathrm{f}^-\rangle + \langle\psi_\mathrm{i}^-|\delta v|\psi_\mathrm{f}^+\rangle + \langle\psi_\mathrm{i}^+|\delta v|\psi_\mathrm{f}^-\rangle + \langle\psi_\mathrm{i}^+|\delta v|\psi_\mathrm{f}^+\rangle \tag{2.12}$$

is depicted in Figure 2.1. It can be written in an obvious shorthand notation

$$\langle\psi_\mathrm{i}|\delta v|\psi_\mathrm{f}\rangle = \sum_{\pm_\mathrm{i}}\sum_{\pm_\mathrm{f}}\langle\psi_\mathrm{i}^\pm|\delta v|\psi_\mathrm{f}^\pm\rangle\,. \tag{2.13}$$

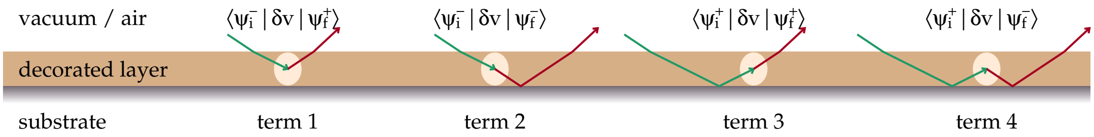

Figure 2.1: The four terms in the DWBA scattering matrix element (2.13). Note that this is a highly simplified visualization. In particular, it does not show multiple reflections of incoming or scattered radiation, though they are properly accounted for by DWBA theory and by all simulation software.

This equation contains the essence of the DWBA for GISAS, and is the base for all scattering models implemented in BornAgain. Since $\langle \psi_\mathrm{i} | \delta v | \psi_\mathrm{f} \rangle$ appears as a squared modulus in the differential cross section (1.30), the four terms of (2.13) can interfere with each other, which adds to the complexity of GISAS patterns.

BornAgain supports multilayer samples with refractive index discontinuities at layer interfaces. Conventions for layer numbers and interface coordinates are introduced in Figure 2.2. A sample has N layers, including the semi-infinite bottom and top layers. Numbering is from top to bottom, and from 0 to $N-1$ as imposed by the programming languages C++ and Python. Each layer l has a constant refractive index n_l and a constant wavenumber $k_l := K_\mathrm{vac} n_l$. Any up- or downward travelling solution of the wave equation shall be written as a sum over partial wavefunctions,

$$\psi^\pm(\mathbf{r}) = \sum_l \psi_l^\pm(\mathbf{r}), \tag{2.14}$$

with the requirement

$$\psi_l^\pm(\mathbf{r}) = 0 \text{ for } \mathbf{r} \text{ outside layer } l. \tag{2.15}$$

The DWBA matrix element (2.13) then takes the form

$$\langle \psi_\mathrm{i} | \delta v | \psi_\mathrm{f} \rangle = \sum_l \sum_{\pm_\mathrm{i}} \sum_{\pm_\mathrm{f}} \langle \psi_{\mathrm{i}l}^\pm | \delta v | \psi_{\mathrm{f}l}^\pm \rangle \,. \tag{2.16}$$

2.1.3 DWBA for layers with constant mean SLD

We now specialize to the case that $\overline{v}(z)$ is a step function: within each layer, $\overline{v}(z) =: v_l$ is constant. Accordingly, within the layer, the directional neutron wavefunction $\psi_l^\pm$ is a plane wave and factorizes as in (2.9). Its amplitude $A_l^\pm$ is determined recursively by Fresnel's transmission and reflection coefficients that are based on continuity conditions at the layer interfaces. This will be elaborated in Section 2.1.4. The vertical wavenumber is determined by (2.3) and (2.5),

$$\kappa_l^\pm = \pm\sqrt{k_l^2 - k_\parallel^2}. \tag{2.17}$$

In the absence of absorption and above the critical angle, wavevectors are real so that we can describe the beam in terms of a glancing angle

$$\alpha_l := \arctan(\kappa_l / k_\parallel). \tag{2.18}$$

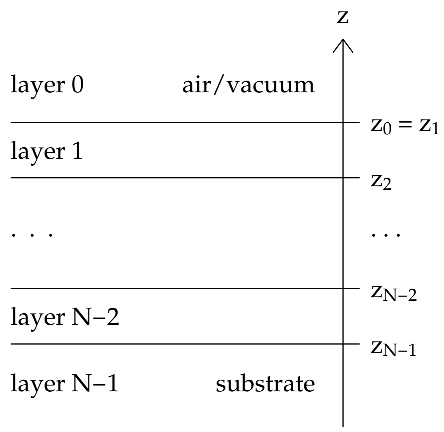

Figure 2.2: Conventions for layer numbers and interface coordinates. A sample has N layers, including the semi-infinite bottom and top layers. Layers are numbered from top to bottom. The top vacuum (or air) layer (which extends to $z \to +\infty$) has number 0, the substrate (extending to $z \to -\infty$) is layer $N-1$. The parameter z_l is the z coordinate of the *top* interface of layer l, except for z_0 which is the coordinate of the *bottom* interface of the air or vacuum layer 0.

Equivalently,

$$k_{\|} = K n_l \cos\alpha_l. \tag{2.19}$$

Since $k_{\|}$ is constant across layers, we have

$$n_l \cos\alpha_l = \text{the same for all } l, \tag{2.20}$$

which is Snell's refraction law. In general, however, the vertical wavenumber κ_l, determined by k_l and $k_{\|}$ as per (2.3), can become imaginary (total reflection conditions) or complex (absorbing layer). In these cases, glancing angles are no longer well defined, and the geometric interpretation of $\psi_l(\mathbf{r})$ less obvious. so that one has to fully rely on the algebraic formalism.

With the indicator function

$$\chi_l(\mathbf{r}) := \begin{cases} 1 & \text{if } z_l \le z \le z_{l+1}, \\ 0 & \text{otherwise,} \end{cases} \tag{2.21}$$

the vertical wavefunction can be written

$$\phi_l^{\pm}(z) = A_l^{\pm} \mathrm{e}^{\pm i\kappa_l (z-z_l)} \chi_l(z). \tag{2.22}$$

The offset z_l has been included in the phase factor for later convenience.

The DWBA transition matrix element (2.13) is

$$\langle\psi_\mathrm{i}|\delta v|\psi_\mathrm{f}\rangle = \sum_l \sum_{\pm_\mathrm{i}} \sum_{\pm_\mathrm{f}} A_{\mathrm{i}l}^{\pm *} A_{\mathrm{f}l}^{\pm} \delta v_l(\mathbf{k}_{\mathrm{f}l}^{\pm} - \mathbf{k}_{\mathrm{i}l}^{\pm}) \tag{2.23}$$

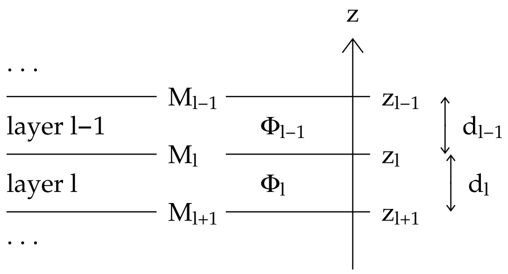

Figure 2.3: The transfer matrix M_l connects the wavefunctions Φ_l, Φ_{l-1} in adjacent layers.

with the Fourier transform of the SLD restricted to layer l

$$\delta v_l(\mathbf{q}) := \int_{z_l}^{z_{l-1}} \mathrm{d}z \int \mathrm{d}^2 r_{\|}\, \mathrm{e}^{i\mathbf{q}\mathbf{r}} \delta v(\mathbf{r}) = \int \mathrm{d}^3 r\, \mathrm{e}^{i\mathbf{q}\mathbf{r}} \delta v(\mathbf{r}) \chi_l(z). \tag{2.24}$$

To alleviate later calculations, we number the four DWBA terms from 1 to 4 as shown in Fig. 2.1, and define the corresponding wavenumbers and amplitude factors and as

$$\begin{aligned}
\mathbf{q}^1 &:= \mathbf{k}_\mathrm{f}^+ - \mathbf{k}_\mathrm{i}^-, & C^1 &:= A_\mathrm{i}^{-*} A_\mathrm{f}^+,\\
\mathbf{q}^2 &:= \mathbf{k}_\mathrm{f}^- - \mathbf{k}_\mathrm{i}^-, & C^2 &:= A_\mathrm{i}^{-*} A_\mathrm{f}^-,\\
\mathbf{q}^3 &:= \mathbf{k}_\mathrm{f}^+ - \mathbf{k}_\mathrm{i}^+, & C^3 &:= A_\mathrm{i}^{+*} A_\mathrm{f}^+,\\
\mathbf{q}^4 &:= \mathbf{k}_\mathrm{f}^- - \mathbf{k}_\mathrm{i}^+, & C^4 &:= A_\mathrm{i}^{+*} A_\mathrm{f}^-.
\end{aligned} \tag{2.25}$$

Accordingly, we can write (2.23) as

$$\langle \psi_\mathrm{i} | \delta v | \psi_\mathrm{f} \rangle = \sum_l \sum_u C_l^u \delta v_l(\mathbf{q}_l^u). \tag{2.26}$$

Since $\mathbf{k}_{\|} = \text{const}$, all wavevectors $\mathbf{q}_l^u$ have the same horizontal component $\mathbf{q}_{\|}$; they differ only in their vertical component $q_{l\perp}^u$.

2.1.4 Wave amplitudes

The plane-wave amplitudes $A_{wl}^{\pm}$ need to be computed recursively from layer to layer. Since these computations are identical for incident and final waves, we omit the subscript w in the remainder of this section. At layer interfaces, the optical potential changes discontinuously. From elementary quantum mechanics we know that piecewise solutions of the Schrödinger equations must be connected such that the wavefunction $\phi(\mathbf{r})$ and its first derivative $\nabla\phi(\mathbf{r})$ evolve continuously.

To deal with the coordinate offsets introduced in (2.22), we introduce the function

$$d_l := z_l - z_{l+1}, \tag{2.27}$$

which is the thickness of layer l, except for $l = 0$, where the special definition of z_0 (Fig. 2.2) implies $d_0 = 0$. We consider the interface between layers l and $l-1$, with $l = 1, \ldots, N-1$, as shown in Fig. 2.3. This interface has the vertical coordinate $z_l = z_{l-1} - d_{l-1}$. Accordingly, the continuity conditions at the interface are

$$\begin{aligned} \phi_l(z_l) &= \phi_{l-1}(z_{l-1} - d_{l-1}), \\ \partial_z \phi_l(z_l) &= \partial_z \phi_{l-1}(z_{l-1} - d_{l-1}). \end{aligned} \tag{2.28}$$

We define the phase factor

$$\delta_l := \mathrm{e}^{i\kappa_l d_l}. \tag{2.29}$$

Here and in the following, we will write the downward travelling transmitted and of the upward travelling reflected amplitude as

$$t_l := A_l^- \quad \text{and} \quad r_l := A_l^+. \tag{2.30}$$

For the plane waves (2.22), the continuity conditions (2.28) take the form

$$\begin{aligned} t_l \quad + r_l &= \delta_{l-1} t_{l-1} \qquad + \delta_{l-1}^{-1} r_{l-1}, \\ -\kappa_l t_l + \kappa_l r_l &= -\kappa_{l-1}\delta_{l-1} t_{l-1} + \kappa_{l-1}\delta_{l-1}^{-1} r_{l-1}. \end{aligned} \tag{2.31}$$

After some lines of linear algebra, we can rewrite this equation system as

$$\begin{pmatrix} t_{l-1} \\ r_{l-1} \end{pmatrix} = M_l \begin{pmatrix} t_l \\ r_l \end{pmatrix} \tag{2.32}$$

with the transfer matrix[1]

$$M_l := \Delta_{l-1} S_l, \tag{2.33}$$

which we write using the phase rotation matrix

$$\Delta_l := \begin{pmatrix} \delta_l^{-1} & 0 \\ 0 & \delta_l \end{pmatrix} \tag{2.34}$$

and the refraction matrix

$$S_l := \begin{pmatrix} s_l^+ & s_l^- \\ s_l^- & s_l^+ \end{pmatrix} \tag{2.35}$$

with coefficients

$$s_l^\pm := \frac{1 \pm \kappa_l/\kappa_{l-1}}{2}. \tag{2.36}$$

Energy conservation can be easily verified for real-valued wave numbers. The vertical flux is $J = |\Phi|^2\kappa$. Under the action of either Δ or S,

$$\kappa_l(|t_l|^2 - |r_l|^2) = \text{const for all } l. \tag{2.37}$$

[1] This approach is generally attributed to Abelès, who elaborated it in his thesis from 1949, published 1950. The usually cited paper [11] is no more than a short advertisement.

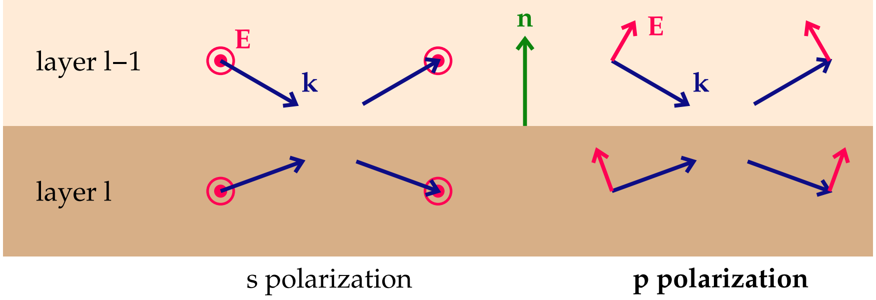

Figure 2.4: Conventions for polarization directions relative to a refracting interface: For s polarization, the electric field vector $\mathbf{E}$ is perpendicular (*senkrecht* in German) to the plane spanned by the interface normal $\mathbf{n}$ and the incoming wavevector $\mathbf{k}$; for p polarization, it is parallel. In either case, $\mathbf{E}$ is perpendicular to $\mathbf{k}$.

2.1.5 Wave amplitudes for X-rays

We shall now translate the above results from unpolarized neutrons to X-rays. The vectorial amplitude of the electromagnetic field will require nontrivial modifications. In place of the factorization (2.9), we write

$$\mathbf{E}(\mathbf{r}) = \mathrm{e}^{i\mathbf{k}_\parallel \mathbf{r}}\mathbf{\Phi}(z). \tag{2.38}$$

In place of (2.22), the vertical wavefunction is

$$\mathbf{\Phi}_l^\pm(z) = \mathbf{A}_l^\pm \mathrm{e}^{\pm i\kappa(z-z_l)}\chi_l(z). \tag{2.39}$$

The vectorial character of $\mathbf{A}_{wl}^\pm$ will require changes with respect to Sec. 2.1.4. For electromagnetic radiation in nonmagnetic media, the boundary conditions at an interface with normal $\mathbf{n}$ are [12, eq. 7.37]

$$\sum_\pm \overline{\epsilon}\,\mathbf{E}^\pm\,\mathbf{n} = \text{const}, \tag{2.40}$$

$$\sum_\pm \mathbf{E}^\pm \times \mathbf{n} = \text{const}, \tag{2.41}$$

$$\sum_\pm \mathbf{k}_l^\pm \times \mathbf{E}^\pm = \text{const}. \tag{2.42}$$

We will only consider the two polarization directions, conventionally designated as p and s, defined in Figure 2.4. As some algebra on (2.40) to (2.42) would show, these are *principal axes*, meaning that if both incoming fields $\mathbf{E}_{l-1}^-$ and $\mathbf{E}_l^+$ are strictly polarized in either s or p direction, then the outgoing fields $\mathbf{E}_{l-1}^+$ and $\mathbf{E}_l^-$ are polarized in the same direction. Conversely, if the incoming fields are mixtures of s and p polarization, then the outgoing fields will be, in general, mixed differently. Therefore if polarization factors are quantitatively important in an experiment, one should strive to accurately polarize the incident beam in s or p direction in order to avoid the extra complication of variably mixed polarizations.

Further algebra on (2.40) to (2.42) replicates the reflection law that relates $\mathbf{k}^-$ and k^+ and Snell's law (2.20). Taking these for granted, we only retain equations that are needed to determine the field amplitudes $E^\pm$. For s polarization they yield

$$\begin{pmatrix} 1 & 1 \\ -\kappa & \kappa \end{pmatrix} \begin{pmatrix} E^- \\ E^+ \end{pmatrix} = \text{const.} \tag{2.43}$$

and for p polarization

$$\begin{pmatrix} n & n \\ -\kappa/n & \kappa/n \end{pmatrix} \begin{pmatrix} E^- \\ E^+ \end{pmatrix} = \text{const,} \tag{2.44}$$

The former equation can be brought into the form (2.31). In consequence, s-polarized X-rays are refracted and reflected in exactly the same ways as unpolarized neutrons.

For p polarization, the refraction matrix coefficients become

$$s_l^\pm = \frac{1}{2}\left(\frac{n_l}{n_{l-1}} \pm \frac{\kappa_l}{\kappa_{l-1}}\frac{n_{l-1}}{n_l}\right) \tag{2.45}$$

instead of (2.36).[2]

2.1.6 Scattering of X-rays

The DWBA matrix element is

$$\langle \mathbf{E}_\text{i}|\delta v|\mathbf{E}_\text{f}\rangle = \sum_l \sum_u C_l^u \delta v_l(\mathbf{q}_l^u). \tag{2.46}$$

in full analogy with (2.26), but the coefficients $C^1 = \mathbf{A}_\text{i}^{-*}\mathbf{A}_\text{f}^+$ etc are now scalar products of vectorial amplitudes. For s polarization all amplitudes point in the same direction, so that we are back to the products of scalar factors of (2.25). For p polarization, incident and scattered field amplitudes point in slightly different directions, which results in correction factors[3]

$$\begin{aligned} C^1 &= A_\text{i}^{-*}A_\text{f}^+ \cos(\alpha_\text{i}^- + \alpha_\text{f}^+), \\ C^2 &= A_\text{i}^{-*}A_\text{f}^- \cos(\alpha_\text{i}^- + \alpha_\text{f}^-), \\ C^3 &= A_\text{i}^{+*}A_\text{f}^+ \cos(\alpha_\text{i}^+ + \alpha_\text{f}^+), \\ C^4 &= A_\text{i}^{+*}A_\text{f}^- \cos(\alpha_\text{i}^+ + \alpha_\text{f}^-). \end{aligned} \tag{2.47}$$

[2] Support for p polarization is not implemented in BornAgain. It can be added easily if there is need.

[3] Also currently not implemented in BornAgain.

2.2 Solution of the split boundary problem

2.2.1 The split boundary problem

We now consider beam propagation through the entire multilayer sample, from the semiinfinite top layer at $l = 0$ to the semiinfinite substrate at $l = N - 1$, which for brevity shall be denoted by $\nu := N - 1$.

Let us assume that the radiation source or sink is located at $z > 0$. Then in the top layer, $t_0 = 1$ is given by the incident or back-traced final plane wave. In the substrate, $t_\nu = 0$ because there is no radiation coming from $z \to -\infty$. This leaves us with two unkown amplitudes, the overall coefficients of transmission t_ν and reflection r_0. These two unknowns are connected by a system of two linear equations,

$$\begin{pmatrix} 1 \\ r_0 \end{pmatrix} = M \begin{pmatrix} t_\nu \\ 0 \end{pmatrix} \tag{2.48}$$

with the matrix product

$$M := M_1 \cdots M_\nu =: \begin{pmatrix} M_{tt} & M_{tr} \\ M_{rt} & M_{rr} \end{pmatrix}. \tag{2.49}$$

To apply this and all the following to the scattered beam in transmission GISAS (sink location $z < 0$), we just reverse the order of layers: $(0, \ldots, \nu) \mapsto (\nu, \ldots, 0)$.

Equation (2.48) is a *split boundary problem* because the given amplitudes $t_0 = 1$, $r_\nu = 0$ appear on different sides of the equation. It can be reorganized as

$$\begin{pmatrix} t_\nu \\ r_0 \end{pmatrix} = W \begin{pmatrix} 1 \\ 0 \end{pmatrix} \tag{2.50}$$

with

$$W = \mathcal{W}(M) := \begin{pmatrix} {M_{tt}}^{-1} & {M_{tt}}^{-1} M_{tr} \\ M_{rt} {M_{tt}}^{-1} & (M_{rr} - M_{rt} {M_{tt}}^{-1} M_{tr}) \end{pmatrix}. \tag{2.51}$$

From (2.50) and (2.51), we can read off

$$t_\nu = M_{tt}^{-1} \quad \text{and} \quad r_0 = M_{rt} M_{tt}^{-1}. \tag{2.52}$$

With this, the split boundary problem is formally solved. However, the matrix product M (2.49) is numerically unstable [13, Sects. III, IV]. Therefore, the actual computation of r_0 and t_ν is done through a recursion (Secs. 2.2.2 and 4.3.1).

If there is one single interface ($\nu = 1$), then $M = S_1$ yields the standard Fresnel results, namely the transmitted amplitude

$$t_1 = \frac{2\kappa_0}{\kappa_0 + \kappa_1} \tag{2.53}$$

and the reflected amplitude

$$r_0 = \frac{\kappa_0 - \kappa_1}{\kappa_0 + \kappa_1}. \tag{2.54}$$

In connection with roughness models, we will need to express the coefficients of the refraction matrix (2.35) through t and r,

$$s_1^+ = \frac{1}{t_1} \quad \text{and} \quad s_1^- = \frac{r_0}{t_1}. \tag{2.55}$$

2.2.2 Recursive solution

As mentioned under (2.52), the matrix product M (2.49) is numerically unstable [13, Sects. III, IV]. It is therefore preferable to solve the split boundary problem through the recursion algorithm of Parratt [14]. It is based on the insight that one does not need to compute t_l and r_l separately, but only their ratio $x_l := r_l/t_l$. Spelling out (2.32) with $\delta := \delta_{l-1}$ and $s^\pm := s_l^\pm$, we obtain

$$x_{l-1} = \frac{\delta s^- + \delta s^+ x_l}{\delta^{-1} s^+ + \delta^{-1} s^- x_l} = \delta^2 \frac{R + x_l}{1 + R x_l}. \tag{2.56}$$

The second expression involves the single-interface Fresnel reflection coefficient

$$R := \frac{s^-}{s^+} = \frac{\kappa_{l-1} - \kappa_l}{\kappa_{l-1} + \kappa_l}. \tag{2.57}$$

The recursion starts at the bottom with $x_\nu = 0$.

2.3 Implementation

Last updated to reflect the actual code in May 2023.

2.3.1 Call chain

All simulations are run through the virtual function `ISimulation::runComputation`.

For classes `ScatteringSimulation` and `OffspecSimulation`,
most work is done in `Compute::scattered_and_reflected`,

for class `SpecularSimulation` in `Compute::reflectedIntensity`,

whereas class `DepthprobeSimulation` performs the computation directly in `runComputation`.

In function `Compute::scattered_and_reflected`,
incoming and outgoing fluxes are obtained from functions `ReSample::fluxesIn` and `fluxesOut`,
and stored in instances of class `Fluxes`, which incarnates `OwningVector<IFlux>`.
Following that, scattering is computed by functions `Compute::dwbaContribution` and
`Compute::roughMultiLayerContribution`.
Specular intensity is added to the appropriate detector pixel by function
`Compute::gisasSpecularContribution`.

In `DepthprobeSimulation::runComputation`, incoming fluxes are obtained from function
`ReSample::fluxesIn`.

In functions `ReSample::fluxesIn` and `fluxesOut` call either `Compute::SpecularScalar::fluxes` or `Compute::SpecularMagnetic::fluxes`.

For specular simulations, function `Compute::reflectedIntensity` calls either `Compute::SpecularScalar::topLayerR` or `Compute::SpecularMagnetic::topLayerR`. These functions only return amplitudes reflected from the top of the sample, whereas the `fluxes` functions called for scattering or depthprobe simulation compute up and down travelling amplitudes for each sample layer.

Functions `fluxes` and `topLayerR` are implemented in files ComputeFluxScalar.cpp and ComputeFluxMagnetic.cpp, where they share some local functions.

2.3.2 Scalar fluxes

The core numeric algorithm for the scalar flux computation is implemented in ComputeFluxScalar.cpp. Here the code is simplified by omitting roughness and transmission geometry. The code uses class `Spinor`, which has components `u` and `v`, here representing transmitted and reflected amplitude. Interfaces are numbered as in Fig. 2.2.

```
std::vector<Spinor>
computeTR(SliceStack& slices, std::vector<cmplx>& kz)
{
    // Parratt algorithm, pass 1:
    //    compute t/t factors and r/t ratios from bottom to top.
    size_t N = slices.size();
    std::vector<cmplx> tfactor(N-1); // transmission damping
    std::vector<cmplx> ratio(N);     // Parratt's x=r/t
    ratio[N-1] = 0;
    for (size_t i = N-1; i > 0; i--) {
        cmplx slp = 1 + kz[i]/kz[i-1];
        cmplx slm = 1 - kz[i]/kz[i-1];
        cmplx delta = exp_I(kz[i-1] * slices[i-1].thicknessOr0());
        cmplx f = delta / (slp + slm * ratio[i]);
        tfactor[i-1] = 2 * f;
        ratio[i-1] = delta * (slm + slp * ratio[i]) * f;
    }

    // Parratt algorithm, pass 2:
    //    compute r and t from top to bottom.
    std::vector<Spinor> TR(N);
    TR[0] = Spinor(1., ratio[0]);
    for (size_t i = 1; i < N; ++i) {
        TR[i].u = TR[i-1].u * tfactor[i-1]; // Spinor.u is t
        TR[i].v = ratio[i] * TR[i].u;       // Spinor.v is r
    }

    return TR;
}
```

The are two code blocks, each with a loop over interfaces. The first loop runs from bottom $l = \nu$ to top $l = 1$. Variables `slp` and `slm` are the coefficients $s_l^\pm$ of (2.36). Variable `delta` is δ_{l-1} as defined in (2.29). These are used for recursively computing transmission damping factors

$$h_{l-1} := \frac{2\delta_{l-1}}{s_l^+ + s_l^- x_l} \tag{2.58}$$

and Parratt ratios (2.56)

$$x_{l-1} = \delta_{l-1} \frac{s_l^- + s_l^+ x_l}{2} h_{l-1} = \delta_{l-1}^2 \frac{s_l^- + s_l^+ x_l}{s_l^+ + s_l^- x_l}, \tag{2.59}$$

starting from the bottom value $x_\nu = 0$. The second loop starts from the top where $t_0 = 1$, $r_0 = 0$. From (2.32),

$$t_{l-1} = \delta^{-1} \left(s^+ t_l + s^- r_l \right) = \frac{s^+ + s^- x_l}{\delta} t_l = h_{l-1}^{-1} t_l. \tag{2.60}$$

Bringing h_{l-1} to the other side, we obtain code line 24. By definition, $x_l = r_l / t_l$. Bringing t_l to the other side, we obtain code line 25.

3 Rough interfaces

The SLD decomposition (2.1) leaves some freedom how to model interface roughness. In the standard approach, $\overline{v}(z)$ always represents the average SLD at given height z. Insofar, roughness has the same effect as an SLD gradient in a sample that is translationally invariant in the xy plane. The effect of graded SLD profiles upon reflection and transmission of a multilayer sample is discussed in Sec. 3.1.

Additionally, the horizontal inhomogeneity of a rough interface gives rise to diffuse scattering, discussed in Sec. 3.2.

By energy conservation, scattering reduces the reflected or/and transmitted intensity. How to account for these losses in the R/T computation is an open research question.

3.1 Propagation through graded interfaces

3.1.1 Interface with tanh profile

Graded interfaces have a smooth SLD profile, i.e. the function $\overline{v}(z)$ or $\kappa^2(z)$ evolves continuously from one bulk value to the other. Among the SLD profiles that can be solved analytically, the tanh (Fig. 3.1a) profile is particularly important. A good summary of the solution can be found in Ch. 2.5 of Lekner [15].[1] Whereas Lekner only considers the electromagnetic case with a profile $\epsilon(z)$, we summarize the theory in terms of $\kappa = \epsilon K^2 - k_\parallel^2$.

We posit a profile

$$\kappa^2(z) = \frac{\kappa_a^2 + \kappa_b^2}{2} + \frac{\kappa_b^2 - \kappa_a^2}{2} \tanh\frac{z}{2\tau}. \tag{3.1}$$

The parameter τ is related to the roughness vertical length parameter σ of the BornAgain API through

$$\pi\tau = \left(\frac{\pi}{2}\right)^{3/2}\sigma. \tag{3.2}$$

For reference, we note the derivative

$$\frac{\mathrm{d}}{\mathrm{d}z}\kappa^2(z) = \frac{\kappa_b^2 - \kappa_a^2}{4\tau}\cosh^{-2}\frac{z}{2\tau}. \tag{3.3}$$

[1] He credits Eckart (1930) and Epstein (1930) for the solution. For a short summary, see also [16, § 25, exercise 3].

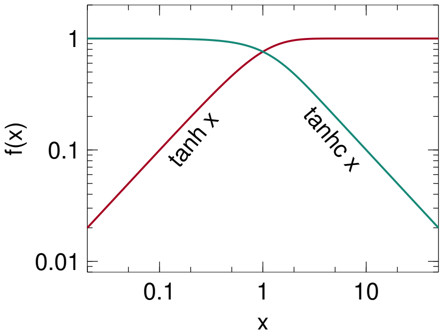

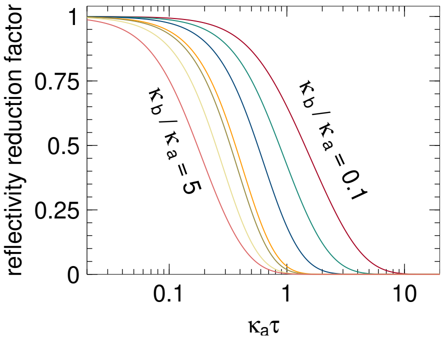

Figure 3.1: (a) Functions tanh and tanhc. (b) Reflectivity reduction factor, obtained by dividing (3.7) through the Fresnel reflectivity (2.53), as function of $\kappa_a\tau$ for ratios κ_b/κ_a of 0.1, 0.2, 0.4, 0.9, 1.1, 2, and 5.

The solution $\Phi(z)$ involves a hypergeometric function. Here we only note the reflection coefficient [15, Eq. 2.88]

$$r_{ab} = \mathrm{e}^{2i\varphi}\frac{\sinh\pi\tau(\kappa_a-\kappa_b)}{\sinh\pi\tau(\kappa_a+\kappa_b)}. \tag{3.4}$$

The phase φ is a real number as long as κ_a and κ_b are real. The transmission coefficient t_{ab} is communicated in [17]. Using various properties of the Gamma and sinh functions, one can verify flux conservation (2.37).

In the limit $\tau \to 0$, the phase factor φ in (3.4) goes to zero. For simplicity, we let $\varphi = 0$ throughout. This approximation is equivalent to an adjustment of the interface position z_{ab} by an amount that can be expected to be small compared to the interface thickness τ_{ab}.

To rewrite (3.4) in a form inspired by the Fresnel reflection coefficient (2.54), we use the identity

$$\frac{\sinh(x-y)}{\sinh(x+y)} = \frac{\sinh x\cosh y - \sinh y\cosh x}{\sinh x\cosh y + \sinh y\cosh x} = \frac{\tanh y - \tanh x}{\tanh y + \tanh x} \tag{3.5}$$

with $x \coloneqq \pi\tau\kappa_a$ and $y \coloneqq \pi\tau\kappa_b$. We write $\operatorname{tanhc} x \coloneqq (\tanh x)/x$ (Fig. 3.1a) and define the roughness factor

$$\mathcal{R}_{ab} \coloneqq \sqrt{\frac{\operatorname{tanhc}\pi\tau\kappa_b}{\operatorname{tanhc}\pi\tau\kappa_a}}. \tag{3.6}$$

With all this, (3.4) can be cast as

$$r_{ab} = \frac{\mathcal{R}_{ab}^{-1}\kappa_a - \mathcal{R}_{ab}\kappa_b}{\mathcal{R}_{ab}^{-1}\kappa_a + \mathcal{R}_{ab}\kappa_b}, \tag{3.7}$$

which has the form of the Fresnel reflection coefficient (2.54), except for the factors $\mathcal{R}_{ab}^{-1}$ and $\mathcal{R}_{ab}$. For $\tau \to 0$, these factors go to 1 so that (2.54) is fully recovered (Fig. 3.1b).

The reduced r_{ab} of (3.7) can be obtained from the basic transfer matrix equation (2.32) if the coefficients $s^\pm$ of (2.36) are replaced by[2]

$$s_a^\pm = \mathcal{R}_{ab}^{-1} \pm \mathcal{R}_{ab}\kappa_b/\kappa_a. \tag{3.8}$$

It is easily verified that the energy conservation (2.37) still holds.

3.1.2 Névot-Croce factor

The Névot-Croce factor is an exponential attenuation factor for the reflection coefficient:

$$\tilde{r}_{ab} = r_{ab}\,\mathrm{e}^{-2k_a k_b \sigma_{ab}^2}, \tag{3.9}$$

where r_{ab} is the Fresnel reflectivity (2.54) of a sharp interface. This form can be obtained in various ways, with more or less hand-wavy arguments or approximations. As e.g. used by Tolan it can be obtained by averaging the Parrat recursion equations over a Gaussian material profile [18], equation 2.34. The same result can also be obtained from formal perturbation theory, see e.g. [19] and references therein.

If the transmission coefficients are left unaltered, the resulting reduction in reflectivity can be interpreted as a loss into diffuse scattering channels. This interpretation is mentioned by Névot et al. [20].

More questionable is the simultaneous modification of the transmission coefficient. Currently BornAgain uses

$$\tilde{t}_{ab} = t_{ab}\,\mathrm{e}^{+(k_a-k_b)^2\sigma^2/2}, \tag{3.10}$$

where t_{ab} is the Fresnel coefficient (2.53). This is the result obtained by Tolan [18, Eq. 2.35], and is also given by de Boer [19] as a result from formal perturbation theory in the limit of very small lateral correlation length. To obtain $\tilde{r}_{ab}$ and $\tilde{t}_{ab}$ from the basic transfer matrix equation (2.32), we need to replace the coefficients $s^\pm$ of (2.36) by

$$s_l^\pm = (1 \pm \kappa_{l-1}/\kappa_l)\exp(-(\kappa_{l-1} \mp \kappa_l)^2\sigma^2/2), \tag{3.11}$$

which is consistent with [21, Eq. 3.114].

However, the total reflected and transmitted flux $\kappa_a|\tilde{r}_{ab}|^2 + \kappa_b|\tilde{t}_{ab}|^2$, computed as in (2.37), is *greater* than the incoming flux κ_a. This takes all credibility from (3.10) and (3.11).

3.2 Scattering by a rough interface

...

[2]Implemented in file ComputeFluxScalar.cpp, function `transition` [30may23].

4 Polarized wave propagation and scattering

In this chapter, we generalize our treatment of wave propagation and grazing-incidence small-angle scattering to polarized neutrons. We therefore need to study spinor wave equations, in contrast to the scalar theory of the previous chapters.

4.1 Polarized neutrons in 2+1 dimensions

4.1.1 Schrödinger equation for neutron spinors

In presence of a magnetic field,[1] the propagation of free neutrons becomes spin dependent. Therefore the scalar wavefunction of Sec. 1.1.1 must be replaced by the spinor[2]

$$\Psi(\mathbf{r}) = \begin{pmatrix} \psi_{z+}(\mathbf{r}) \\ \psi_{z-}(\mathbf{r}) \end{pmatrix}. \tag{4.1}$$

The coupling between the neutron and the $\mathbf{B}$ field is given by the operator $-\gamma_\mathrm{n}\mu_\mathrm{nucl}\mathbf{B}\breve{\boldsymbol{\sigma}}$ with the neutron gyromagnetic factor $\gamma_\mathrm{n} \simeq -1.91$, the nuclear magnetron μ_nucl, and the Pauli vector $\breve{\boldsymbol{\sigma}}$, composed of the three Pauli matrices (the *breve* diacritic denotes an operator in spin space, represented by a complex 2×2 matrix). With the unsigned magnetic moment of the neutron, $\mu_\mathrm{n} \coloneqq |\gamma_\mathrm{n}\mu_\mathrm{nucl}|$, the Schrödinger equation (1.1) becomes

$$\left\{-\frac{\hbar^2}{2m}\nabla^2 + V(\mathbf{r}) + \mu_\mathrm{n}\mathbf{B}(\mathbf{r})\breve{\boldsymbol{\sigma}} - \hbar\omega\right\}\Psi(\mathbf{r}) = 0. \tag{4.2}$$

Except near Bragg reflections, $\mathbf{B}$ is an averaged, macroscopic field [24], just like V is an averaged potential (1.6).

We abbreviate the nuclear and the magnetic scattering-length density as

$$\rho^\mathrm{N}(\mathbf{r}) \coloneqq v_\mathrm{nucl}(\mathbf{r}) \quad \text{and} \quad \rho^\mathrm{M}(\mathbf{r}) \coloneqq \frac{m\mu_\mathrm{n}}{2\pi\hbar^2}B(\mathbf{r}), \tag{4.3}$$

and we write $\hat{\mathbf{B}}$ for the unit vector in direction of the magnetic field $\mathbf{B}$. So the total reduced potential is given by the operator

$$\breve{v}(\mathbf{r}) \coloneqq \rho^\mathrm{N}(\mathbf{r}) + \rho^\mathrm{M}(\mathbf{r})\hat{\mathbf{B}}(\mathbf{r})\breve{\boldsymbol{\sigma}}, \tag{4.4}$$

[1] According to Ref. [22], the magnetic field is usually applied parallel to the sample surface, but we do not rely on this.

[2] Spinors can also be used to describe polarized X-rays [23]. Please let us know if there is a use case for BornAgain.

and we can rewrite the Schrödinger equation in analogy to (4.5) as

$$\left\{\nabla^2 + K^2 - 4\pi\breve{v}(\mathbf{r})\right\}\Psi(\mathbf{r}) = 0. \tag{4.5}$$

4.1.2 Propagation in a multilayer

In the decomposition (2.1), both terms may become operators acting in spin space,

$$\breve{v}(\mathbf{r}) =: \breve{\overline{v}}(z) + \delta\breve{v}(\mathbf{r}). \tag{4.6}$$

The unperturbed distorted wave has the form

$$\Phi(\mathbf{r}) = \mathrm{e}^{i\mathbf{k}_\parallel\mathbf{r}_\parallel}\Phi(z). \tag{4.7}$$

The horizontal wave vector $\mathbf{k}_\parallel$ is constant across layers. This motivates us to introduce the vertical vacuum wavenumber $\kappa_0 := \sqrt{K^2 - k_\parallel^2}$. The vertical spinor wave function $\Phi(z)$ obyes the equation

$$\left\{\nabla^2 + \kappa_0^2 - 4\pi\breve{\overline{v}}(z)\right\}\Phi(z) = 0. \tag{4.8}$$

In absence of a magnetic field, $\overline{v}(z)$ is scalar (or proportional to the unit matrix $\breve{1}$), and each spinor component will propagate exactly as in the scalar case of Sec. 2.1. Conversely, if there is a nonzero magnetic field, then the neutron spin will undergo Larmor precession, which in spinor representation shows up as oscillations between the two spinor components. In consequence, when an incident plane wave hits a magnetic medium it becomes a superposition of two plane waves that propagate with two different vertical wavenumbers that correspond to the two eigenvalues of (4.8).

We now consider a homogeneous layer with constant potential. Similar to [25, 26], we write the formal solution of (4.8) as

$$\Phi(z) = \mathrm{e}^{-i\breve{\kappa}z}T + \mathrm{e}^{i\breve{\kappa}z}R, \tag{4.9}$$

where T and R are the transmitted and reflected spinor amplitudes. By comparison with (4.8), we see that the square of the operator $\breve{\kappa}$ is

$$\breve{\kappa}^2 = \kappa_0^2 - 4\pi\breve{\overline{v}} = \kappa_0^2 - 4\pi(\rho^{\mathrm{N}} + \rho^{\mathrm{M}}\hat{\mathbf{B}}\breve{\boldsymbol{\sigma}}). \tag{4.10}$$

4.1.3 Wavenumber operator $\breve{\kappa}$

Without derivation,[3] we state that the square root of $\breve{\kappa}^2$ is the operator

$$\breve{\kappa} = \frac{1}{2}\left[(c_+ + c_-) + (c_+ - c_-)\hat{\mathbf{B}}\breve{\boldsymbol{\sigma}}\right], \tag{4.11}$$

[3] To verify, use standard properties of Pauli matrices. Square (4.11) to reproduce (4.10). Then confirm that $c_\pm^2$ are eigenvalues of $\breve{\kappa}^2$. See also [16, § 55, Exercice 1, p. 198].

expressed through its eigenvalues

$$c_\pm \coloneqq \sqrt{\kappa_0^2 - 4\pi\rho^{\mathrm{N}} \pm 4\pi\rho^{\mathrm{M}}}. \tag{4.12}$$

With the abbreviations

$$\alpha \coloneqq c_+ + c_-, \quad \beta \coloneqq c_+ - c_-, \quad \text{and} \quad \mathbf{b} \coloneqq \beta\hat{\mathbf{B}}, \tag{4.13}$$

we obtain the matrix components[4]

$$\breve{\kappa} = \frac{1}{2}\left(\alpha + \mathbf{b}\breve{\boldsymbol{\sigma}}\right) = \frac{1}{2}\begin{pmatrix} \alpha + b_z & b_x - ib_y \\ b_x + ib_y & \alpha - b_z \end{pmatrix}. \tag{4.14}$$

For future reference, we note the inverse operator[5]

$$\breve{\kappa}^{-1} = \frac{1}{2c_+c_-}\left[(c_+ + c_-) - (c_+ - c_-)\hat{\mathbf{B}}\breve{\boldsymbol{\sigma}}\right] \tag{4.15}$$

$$= \frac{2}{\alpha^2 - \beta^2}(a - \mathbf{b}\breve{\boldsymbol{\sigma}}) \tag{4.16}$$

$$= \frac{2}{\alpha^2 - \beta^2}\begin{pmatrix} \alpha - b_z & -b_x + ib_y \\ -b_x - ib_y & \alpha + b_z \end{pmatrix}. \tag{4.17}$$

It does not exist if ρ^{N} is real and $\rho^{\mathrm{M}} = \kappa_0^2/(4\pi) - \rho^{\mathrm{N}}$. If ρ^{M} is even larger, then $\breve{\kappa}$ becomes pure imaginary, causing evanescent waves, to be discussed later (Chapter 5).

4.1.4 Eigendecomposition of $\breve{\kappa}$

To evaluate functions of the operator $\breve{\kappa}$, we will need its eigenvalue decomposition. We start with the matrix $\hat{\mathbf{B}}\breve{\boldsymbol{\sigma}}$, which has the eigenvalues ± 1 and the normalized eigenspinors

$$V_1 = \frac{1}{\sqrt{2(1+\hat{B}_z)}}\begin{pmatrix} 1 + \hat{B}_z \\ \hat{B}_x + i\hat{B}_y \end{pmatrix}, \quad V_2 = \frac{1}{\sqrt{2(1+\hat{B}_z)}}\begin{pmatrix} \hat{B}_x - i\hat{B}_y \\ -1 - \hat{B}_z \end{pmatrix}. \tag{4.18}$$

For readability, we have omitted the subscript $\mathbf{B}$ from the components of $\hat{\mathbf{B}}$. and the same eigenvectors as $\hat{\mathbf{B}}\breve{\boldsymbol{\sigma}}$. We introduce the eigenvector matrix

$$\breve{Q}(\mathbf{B}) \coloneqq (V_1, V_2) = \frac{1}{\sqrt{2(1+\hat{B}_z)}}\begin{pmatrix} 1 + \hat{B}_z & \hat{B}_x - i\hat{B}_y \\ \hat{B}_x + i\hat{B}_y & -1 - \hat{B}_z \end{pmatrix}. \tag{4.19}$$

[4] Currently (jun23) implemented in function `MatrixFlux::computeKappa()`.
[5] Currently (jun23) implemented in function `MatrixFlux::computeInverseKappa()`.

The normalization factor becomes singular for $\hat{B}_z = -1$. In this case, the matrix $\hat{\mathbf{B}}\breve{\boldsymbol{\sigma}}$ is just $\breve{\sigma}_z$ and has eigenvectors $V_1 = (1,0)^\dagger$ and $V_2 = (0,1)^\dagger$. Furthermore, we need to take care of the case $\mathbf{B} = 0$. Altogether, we let

$$\breve{Q}(\mathbf{B}) := \begin{cases} \breve{\mathbb{1}} & \text{if } B = 0, \\ \breve{\sigma}_x & \text{if } B_z = -B, \\ (\hat{\mathbf{B}} + \hat{\mathbf{z}})\breve{\boldsymbol{\sigma}} / \sqrt{2(1+\hat{B}_z)} & \text{else.} \end{cases} \tag{4.20}$$

The matrix $\breve{\kappa}$ has the eigenvalues $c_\pm$, and the same eigenvectors as $\hat{\mathbf{B}}\breve{\boldsymbol{\sigma}}$. Accordingly, it has the eigendecomposition

$$\breve{\kappa} = \breve{Q} \begin{pmatrix} c_+ & 0 \\ 0 & c_- \end{pmatrix} \breve{Q}^\dagger, \tag{4.21}$$

and any holomorphic function $f(\breve{\kappa})$ can be computed as[6]

$$f(\breve{\kappa}) = \breve{Q} \begin{pmatrix} f(c_+) & 0 \\ 0 & f(c_-) \end{pmatrix} \breve{Q}^\dagger. \tag{4.22}$$

4.2 Refraction and reflection at interfaces

4.2.1 Transfer matrix

To match solutions at layer interfaces, we use the transfer matrix method introduced in Sec. 2.1.4. That section was formulated in such ways that only minimal modifications are needed now. Instead of the vertical wave function $\phi(z)$ and the amplitudes t and r, we now have the spinors $\Phi(z)$, T, and R. Instead of the vertical wavenumber $\kappa \equiv k_\perp$ (2.6), we have the operator $\breve{\kappa}$. The phase factor δ (2.29) also becomes an operator,

$$\breve{\delta}_l := \mathrm{e}^{i\breve{\kappa}_l d_l}. \tag{4.23}$$

The equation system (2.32) becomes

$$\begin{pmatrix} T_{l-1} \\ R_{l-1} \end{pmatrix} = \mathbb{M}_l \begin{pmatrix} T_l \\ R_l \end{pmatrix} \tag{4.24}$$

with the 4×4 transfer matrix[7]

$$\mathbb{M}_l := \mathbb{D}_{l-1}\, \mathbb{S}_l \tag{4.25}$$

in place of (2.33). The phase rotation matrix (2.34) is replaced by the block matrix

$$\mathbb{D}_l := \begin{pmatrix} \breve{\delta}_l^{-1} & 0 \\ 0 & \breve{\delta}_l \end{pmatrix}, \tag{4.26}$$

[6] Currently (jun23) implemented in function `MatrixFlux::eigenToMatrix`.
[7] Occasionally called *supermatrix* for being made of 2×2 submatrices [27].

to be discussed in the next section. The refraction matrix (2.35) also is replaced by a block matrix,

$$\mathbb{S}_l := \begin{pmatrix} \breve{s}_l^+ & \breve{s}_l^- \\ \breve{s}_l^- & \breve{s}_l^+ \end{pmatrix} \tag{4.27}$$

with the coefficients[8]

$$\breve{s}_l^\pm := \frac{1 \pm \breve{\kappa}_{l-1}^{-1}\,\breve{\kappa}_l}{2}. \tag{4.28}$$

4.2.2 Phase rotation matrix

With the eigendecomposition (4.22), the phase rotation matrix (4.23) can be written[9]

$$\breve{\delta} = \mathrm{e}^{i\breve{\kappa}d} = \breve{Q}\begin{pmatrix} \mathrm{e}^{idc_+} & 0 \\ 0 & \mathrm{e}^{idc_-} \end{pmatrix}\breve{Q}^\dagger. \tag{4.29}$$

For the analysis of numerical stability, the critical factor $\mathrm{e}^{i\alpha d/2}$ may be drawn in front of $\breve{Q}$ in (4.29),

$$\breve{\delta} = \mathrm{e}^{i\alpha d/2}\breve{Q}\begin{pmatrix} \mathrm{e}^{id\beta/2} & 0 \\ 0 & \mathrm{e}^{-id\beta/2} \end{pmatrix}\breve{Q}^\dagger. \tag{4.30}$$

4.2.3 Interface with tanh profile

In the scalar case, the refraction matrix (2.35) has coefficients (2.36) for a sharp interface, and modified coefficients (3.8) for a graded interface with tanh profile. By analogy, for polarized neutrons the refraction matrix of a sharp interface has matrix blocks (4.28), which for a graded interface with tanh profile are replaced by

$$\breve{s}_a^\pm = \breve{\mathcal{R}}_{ab}^{-1} \pm \breve{\mathcal{R}}_{ab}\breve{\kappa}_b/\breve{\kappa}_a \tag{4.31}$$

with the roughness factor

$$\breve{\mathcal{R}}_{ab} := \sqrt{\operatorname{tanhc}\,\pi\tau\breve{\kappa}_b}/\sqrt{\operatorname{tanhc}\,\pi\tau\breve{\kappa}_a} \tag{4.32}$$

that replaces the scalar factor (3.6). The constant τ, defined in (3.2), is proportional to the vertical roughness length parameter σ. The eigendecomposition (4.22) is applied separately to $\breve{\kappa}_a$ and $\breve{\kappa}_b$ dependent factors,[10]

$$\begin{aligned} \breve{s}_a^\pm &= \breve{Q}_b\begin{pmatrix} 1/h_b^+ & 0 \\ 0 & 1/h_b^- \end{pmatrix}\breve{Q}_b^\dagger\,\breve{Q}_a\begin{pmatrix} h_a^+ & 0 \\ 0 & h_a^- \end{pmatrix}\breve{Q}_a^\dagger \\ &\pm\, \breve{Q}_b\begin{pmatrix} h_b^+c_b^+ & 0 \\ 0 & h_b^-c_b^- \end{pmatrix}\breve{Q}_b^\dagger\,\breve{Q}_a\begin{pmatrix} 1/(h_a^+c_a^+) & 0 \\ 0 & 1/(h_a^-c_a^-) \end{pmatrix}\breve{Q}_a^\dagger \end{aligned} \tag{4.33}$$

with $h^\pm := \sqrt{\operatorname{tanhc}\,\pi\tau c^\pm}$.

[8] Currently (jun23), the matrix blocks $\breve{s}_l^+$ and $\breve{s}_l^-$, possibly modified by roughness factors (see below), are computed through local function `refractionMatrixBlocks` in ComputeFluxMagnetic.cpp.

[9] Currently (jun23) implemented in local function `PhaseRotationMatrix` in file MatrixFlux.cpp.

[10] Currently (jun23) implemented in function `Compute::refractionMatrixBlocksTanh`.

4.2.4 Névot-Croce approximation

To apply the Névot-Croce approximation to polarized neutrons, we rewrite (3.11) in operator form as

$$\breve{s}_a^{\pm} = \frac{1 \pm \breve{\kappa}_b/\breve{\kappa}_a}{2} \exp(-(\breve{\kappa}_b \mp \breve{\kappa}_a)^2\sigma^2/2). \tag{4.34}$$

In contrast to the tanh roughness factor (4.32), the Gaussian factor here does not factorize into separate functions of $\breve{\kappa}_{l-1}$ and $\breve{\kappa}_l$. Therefore we need a dedicated eigendecomposition for the operator

$$\breve{\kappa}^{\pm} := (\breve{\kappa}_b \mp \breve{\kappa}_a)^2 = \frac{1}{2}\left((\alpha^{\pm} \mp \mathbf{b}^{\pm}\breve{\boldsymbol{\sigma}})^2\right) = \frac{1}{4}\left((\alpha^{\pm})^2 + (\mathbf{b}^{\pm})^2 \mp 2\alpha^{\pm}\mathbf{b}^{\pm}\breve{\boldsymbol{\sigma}}\right), \tag{4.35}$$

where

$$\alpha^{\pm} := \alpha_b \mp \alpha_a \quad \text{and} \quad \mathbf{b}^{\pm} := \mathbf{b}_a \mp \mathbf{b}_b. \tag{4.36}$$

Note that we take non-conjugated squares of complex vectors, not squared norms. The eigendecomposition of $\breve{\kappa}^{\pm}$ is computed exactly as for the operator $\breve{\kappa}$ in Sec. 4.1.4.[11]

4.3 Implementation

4.3.1 Generalized Parratt recursion

We now describe the currently implemented solution of the split boundary problem for polarized neutrons. We start from the transfer matrix equation (4.24), which we apply simultaneously to different polarization states. To this end, we replace the spinors T and R by 2×2 matrices $\breve{t}$ and $\breve{r}$:

$$\begin{pmatrix} \breve{t}_{l-1} \\ \breve{r}_{l-1} \end{pmatrix} = \mathbb{M}_l \begin{pmatrix} \breve{t}_l \\ \breve{r}_l \end{pmatrix}. \tag{4.37}$$

To generalize the Parratt recursion, we define

$$\breve{x}_l := \breve{r}_l \breve{t}_l^{-1}. \tag{4.38}$$

With (4.25) to (4.27), we find [27, Eq 65]

$$\begin{aligned} \breve{x}_{l-1} &= \breve{\delta}_{l-1}^2 \left(\breve{s}^-\breve{t} + \breve{s}^+\breve{r}\right)_l \left(\breve{s}^+\breve{t} + \breve{s}^-\breve{r}\right)_l^{-1} & (4.39)\\ &= \breve{\delta}_{l-1}^2 \left(\breve{s}^-\breve{t} + \breve{s}^+\breve{r}\right)_l \breve{t}_l^{-1}\breve{t}_l \left(\breve{s}^+\breve{t} + \breve{s}^-\breve{r}\right)_l^{-1} & (4.40)\\ &= \breve{\delta}_{l-1}^2 \left(\breve{s}^- + \breve{s}^+\breve{x}\right)_l \left(\breve{s}^+ + \breve{s}^-\breve{x}\right)_l^{-1}, & (4.41) \end{aligned}$$

which indeed generalizes the scalar recursion (2.56). This recursive solution is numerically stable, in contrast to the *supermatrix formalism* [28] that solves the split boundary value problem by inversion of $\mathbb{M}$. When modelling specular reflectivity,

[11] Currently (jun23) implemented in function `Compute::refractionMatrixBlocksNevot`.

then it is sufficient to compute the reflected intensity emanating from the top layer. For incident $\breve{t}_0$, the corresponding reflected matrix flux is[12]

$$\breve{r}_0 = \breve{x}_0 \breve{t}_0. \tag{4.42}$$

For a given incident spinor amplitude T_0, the reflected spinor amplitude is

$$R_0 = \breve{x}_0 T_0. \tag{4.43}$$

4.3.2 Fluxes inside the sample

For modelling GISAS, we need the transmitted and reflected fluxes in all layers of the sample. In a first loop we compute the $\breve{x}_l$ from bottom to top as before, and store them all in an array. Then in a second loop we compute the $\breve{t}_l$ and $\breve{r}_l$ from top to bottom.[13]

From (4.37) and (4.38) we have

$$\breve{t}_{l-1} = \breve{\delta}_{l-1}^{-1} \left(\breve{s}^+ + \breve{s}^- \breve{x}\right)_l \breve{t}_l. \tag{4.44}$$

Inverting this, we obtain our recipee for computing transmitted intensities,[14]

$$\breve{t}_l = \breve{\delta}_{l-1} \left(\breve{s}^+ + \breve{s}^- \breve{x}\right)_l^{-1} \breve{t}_{l-1} \tag{4.45}$$

The reflected intensities are then simply

$$\breve{r}_l = \breve{x}_l \breve{t}_l. \tag{4.46}$$

For an efficient implementation, we rearrange (4.41) from the first loop as

$$\breve{x}_{l-1} = \breve{\delta}_{l-1} \left(\breve{s}^- + \breve{s}^+ \breve{x}\right)_l \breve{F}_l \tag{4.47}$$

with matrices

$$\breve{F}_l := \breve{\delta}_{l-1} \left(\breve{s}^+ + \breve{s}^- \breve{x}\right)_l^{-1}, \tag{4.48}$$

which we store to reuse them in the second loop in computing (4.45), which is just

$$\breve{t}_l = \breve{F}_l \breve{t}_{l-1}. \tag{4.49}$$

4.3.3 Numeric stability

...

4.4 Magnetic field

...

[12]Currently (jun23) implemented in function `Compute::polarizedReflectivity`.

[13]Currently (jun23) implemented in function `Compute::polarizedFluxes` and below.

[14]Alternative expressions, involving $\breve{x}_{l-1}$ rather than $\breve{s}^\pm$, can be found in [25, Eq A.3] and [22, Eq 68].

4.5 Density operator formalism

4.5.1 Reflected flux

The density matrix is defined as

$$\breve{\rho} := \sum_A A\, p_A A^+, \tag{4.50}$$

where the spinors A are normalized, but not necessarily orthogonal, and the statistical weights p_A add up to 1. When an operator $\breve{o}$ transforms the A into $\breve{o}A$, then the density operator is transformed into $\breve{o}\breve{\rho}\breve{o}^+$.

A neutron polarizer is described an operator Π that shall not be further specified because it affects observables only through a density operator to be defined below. Under the action of $\breve{\Pi}$, the density matrix of the unpolarized source beam

$$\breve{\rho}_0 := \begin{pmatrix} 1/2 & 0 \\ 0 & 1/2 \end{pmatrix} = \frac{\breve{1}}{2} \tag{4.51}$$

becomes transformed into the density matrix of the polarized incident beam

$$\breve{\rho}_1 = \breve{\Pi}_\mathrm{i}\, \breve{\rho}_0\, \breve{\Pi}_\mathrm{i}^+ = \breve{\Pi}_\mathrm{i}\, \breve{\Pi}_\mathrm{i}^+\, \breve{\rho}_0 \equiv \breve{\rho}_\mathrm{i}\, \breve{\rho}_0. \tag{4.52}$$

In the second equality we used the fact that $\breve{\rho}_0$ is proportional to the unity matrix and therefore commutes with any other matrix. The product of $\breve{\Pi}_\mathrm{i}$ and its conjugate transpose are then combined into the polarizer density operator

$$\breve{\rho}_\mathrm{i} := \breve{\Pi}_\mathrm{i}\, \breve{\Pi}_\mathrm{i}^+. \tag{4.53}$$

In (4.43) we found for a given incident spinor amplitude T a reflected spinor amplitude $\breve{x}_0 T$, where $\breve{x}_0$ is a matrix obtained from the generalized Parratt recursion. Accordingly, the density matrix of the incident beam is transformed into the density matrix of the reflected beam

$$\rho_2 = \breve{x}_0\, \breve{\rho}_1\, \breve{x}^+. \tag{4.54}$$

Finally, the beam is passed through a polarization analyzer and the density matrix becomes

$$\rho_3 = \breve{\Pi}_\mathrm{f}\, \breve{\rho}_2\, \breve{\Pi}_\mathrm{f}^+. \tag{4.55}$$

At this point, the flux is given by the trace

$$I_3 = \mathrm{Tr}\, \breve{\rho}_3 = \mathrm{Tr}\, \breve{\Pi}_\mathrm{f}\, \breve{\rho}_2\, \breve{\Pi}_\mathrm{f}^+ = \mathrm{Tr}\, \breve{\Pi}_\mathrm{f}^+\, \breve{\Pi}_\mathrm{f}\, \breve{\rho}_2 \equiv \mathrm{Tr}\, \breve{\rho}_\mathrm{f}\, \breve{\rho}_2. \tag{4.56}$$

In the second equality we used the invariance of a trace under rotation of matrix factors. In the final identity, we introduced the polarizer density operator

$$\breve{\rho}_\mathrm{f} := \breve{\Pi}_\mathrm{f}^+\, \breve{\Pi}_\mathrm{f}. \tag{4.57}$$

Collecting everything, we obtain[15]

$$I_3 = \frac{1}{2}\, \mathrm{Tr}\, \breve{\rho}_\mathrm{f}\, \breve{x}_0\, \breve{\rho}_\mathrm{i}\, \breve{x}_0^+. \tag{4.58}$$

[15] The leading factor 1/2, which comes from the density matrix (4.51) of the unpolarized source beam, is ignored in BornAgain. Besides that, (4.58) is currently (June 2023) implemented in function `Compute::magneticR` in file SpecularComputation.cpp.

4.5.2 Parameterization of the polarizer density operator

As any other 2×2 matrix, the polarization operator can be written as

$$\breve{\Pi} = p_0\breve{1} + \mathbf{p}\breve{\boldsymbol{\sigma}}, \tag{4.59}$$

and the polarizer density operator as

$$\breve{\rho} = r_0\breve{1} + \mathbf{r}\breve{\boldsymbol{\sigma}}. \tag{4.60}$$

From (4.53) or (4.57), we know that $\breve{\rho} = \breve{\Pi}\,\breve{\Pi}^+$. Inserting (4.59), we can conclude that $\breve{\rho}$ is Hermitean, that r_0 and $\mathbf{r}$ are real, and that $|\mathbf{r}| \le |r_0|$. This allow up to replace (4.60) by

$$\breve{\rho} = \left(\breve{1} + \mathbf{P}\breve{\boldsymbol{\sigma}}\right)\tau. \tag{4.61}$$

We identify $\mathbf{P}$ as the *polarization vector*, and τ as the *mean transmission* of an unpolarized beam; it can take values between 0 and 1/2, whereas the polarization strength $P \coloneqq |\mathbf{P}|$ may take values between 0 and 1. For a source flux I_0, the flux after a beam polarizer has the components

$$I_\pm \coloneqq \mathrm{Tr}(\pm\hat{\mathbf{P}}\breve{\boldsymbol{\sigma}})\breve{\rho}_\mathrm{i}\breve{\rho}_0 I_0 = \frac{1}{2}(1 \pm P)\tau I_0. \tag{4.62}$$

The polarization ratio is

$$\frac{I_+ - I_-}{I_+ + I_-} = P \tag{4.63}$$

in accord with the conventional definition of the polarization degree P [29].

5 Evanescent waves

...

6 Detector models

6.1 Detector images

To conclude this chapter on the foundations of small-angle scattering, we shall derive the geometric factors that allow us to convert differential cross sections into detector counts. We shall also discuss how to present data on a physically meaningful scale.

6.1.1 Pixel coordinates, scattering angles, and q components

We assume that scattered radiation is detected in a flat, two-dimensional detector that generates histograms on a rectangular grid, consisting of $n \cdot m$ pixels of constant width and height, as sketched in Fig. 6.1. This figure also shows the coordinate system according to unanimous GISAS convention, with z normal to the sample plane, and with the incident beam in the xz plane. The origin is at the center of the sample surface. We suppose that the detector is mounted perpendicular to the x axis at a distance L from the sample position. The real-space coordinate at the center of pixel (i, j) is (L, y_i, z_i). Each pixel has a width Δy and a height Δz. BornAgain requires a full parametrization of the detector geometry to correctly perform the affine-linear mapping from pixel indices i, j to pixel coordinates x_i, y_i; see the rectangular detector tutorial.

Since the differential scattering cross section (1.29) is given with respect to a solid-angle element $\mathrm{d}\Omega$, we need to express the scattered wavevector $\mathbf{k}_\mathrm{f}$ in spherical coordinates, using the horizontal azimuth angle ϕ_f and the vertical glancing angle α_f. The projection of $(\alpha_\mathrm{f}, \phi_\mathrm{f})$ into the detector plane (y, z) is known as the *gnomonic projection*. From elementary trigonometry one finds

$$\begin{aligned} y &= L \tan \phi_\mathrm{f}, \\ z &= (L/\cos\phi_\mathrm{f}) \tan \alpha_\mathrm{f}. \end{aligned} \tag{6.1}$$

Fig. 6.2 shows lines of equal α_f, ϕ_f in the detector plane. To emphasize the curvature of the constant-α_f lines, scattering angles up to more than 25° are shown. In typical SAS or GISAS, scattering angles are much smaller, and therefore the mapping between pixel coordinates and scattering angles is in a good first approximation linear. Of course BornAgain is not restricted to this linear regime, but uses the exact nonlinear mapping (6.1).

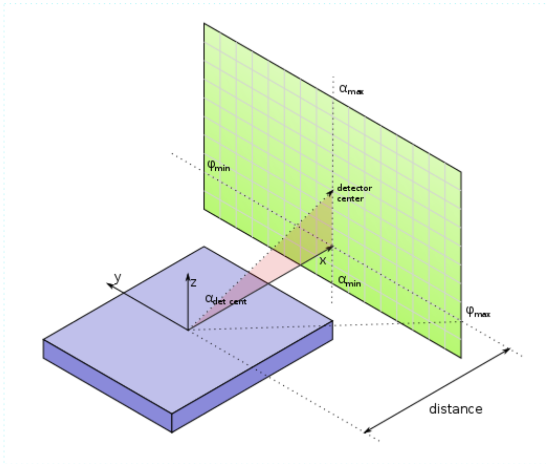

Figure 6.1: Experimental geometry with a two-dimensional pixel detector.

To determine the scattering vector $\mathbf{q}_{ij}$ that corresponds to a pixel (i, j), we need to express the outgoing wavevector $\mathbf{k}_\mathrm{f}$ as function of y and z. This can be done either by inverting (6.1) and inserting the so obtained $\alpha_\mathrm{f}(y, z)$ and $\phi_\mathrm{f}(y)$ in

$$\mathbf{k}_\mathrm{f} = K \begin{pmatrix} \cos\alpha_\mathrm{f}\cos\phi_\mathrm{f} \\ \cos\alpha_\mathrm{f}\sin\phi_\mathrm{f} \\ \sin\alpha_\mathrm{f} \end{pmatrix}, \tag{6.2}$$

or much more directly by using geometric similarity in Cartesian coordinates. The result is rather simple:

$$\mathbf{k}_\mathrm{f} = \frac{K}{\sqrt{L^2 + y^2 + z^2}} \begin{pmatrix} L \\ y \\ z \end{pmatrix}. \tag{6.3}$$

The transform (6.6) between pixel coordinates y, z and physical scattering vector components q_y, q_z is nonlinear, due to the square-root term in the denominator of (6.3). For $y, z \ll L$, however, nonlinear terms loose importance.

The left detector frame in Fig. 6.3 shows circles of constant values of $\pm q_x$. For given steps in q_x, the distance between adjacent circles increases towards the detector center. From (1.33) and (6.3), one finds asymptotically for $y, z \to L$ that q_x goes with the square of the two other components of the scattering vector,

$$\frac{q_x}{K} \doteq \frac{y^2 + z^2}{2L^2} \doteq \frac{q_y^2 + q_z^2}{2K^2}. \tag{6.4}$$

Therefore, under typical small angle conditions $y, z \to L$ the dependence of the scattering signal on q_x is unimportant: one basically measures $v(\mathbf{q}) \simeq v(0, q_y, q_z)$. The exception, for sample structures with long correlations in x direction, is illustrated in Fig. 6.4.

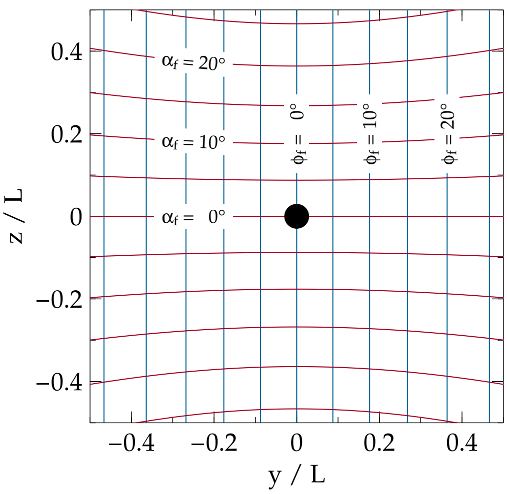

Figure 6.2: Lines of constant α_f (red) or ϕ_f (blue) in the detector plane, for a planar detector at distance L from the sample. The black dot indicates the beamstop location for the central incident beam (SAS geometry, $\breve{\mathbf{k}}_\mathrm{i} = \breve{x}$).

As anticipated in (6.4), the other two components of $\mathbf{q}$ are in first order linear in the pixel coordinates,

$$\frac{q_y}{K} = \frac{y}{L}\left(1 - \frac{y^2+z^2}{2L^2} + \dots\right), \tag{6.5}$$

and similarly for q_z. The nonlinear correction terms lead to the pincushion distortion shown in the right detector frame in Fig. 6.3.

Since pixel coordinates are meaningful only with respect to a specific experimental setup, users may wish to transform detector images towards the physical coordinates q_y and q_z. As shown in Fig. 6.5, this would yield a barrel-shaped illuminated area in the q_y, q_z plane.

To summarize this section, the wavevector $\mathbf{q}_{ij}$ can be determined from the pixel indices through the following steps:

$$\begin{array}{cl} (i,j) & \\ \downarrow & \text{calibrate of origin, then employ affine-linear mapping} \\ (y,z) & \\ \downarrow & \text{use (6.3)} \\ \mathbf{k}_\mathrm{f} & \\ \downarrow & \text{use (1.33)} \\ \mathbf{q} & \end{array} \tag{6.6}$$

Transforming detector images from pixel coordinates into the q_y, q_z plane is not implemented in BornAgain, and not on our agenda. We would, however, like to hear about use cases.

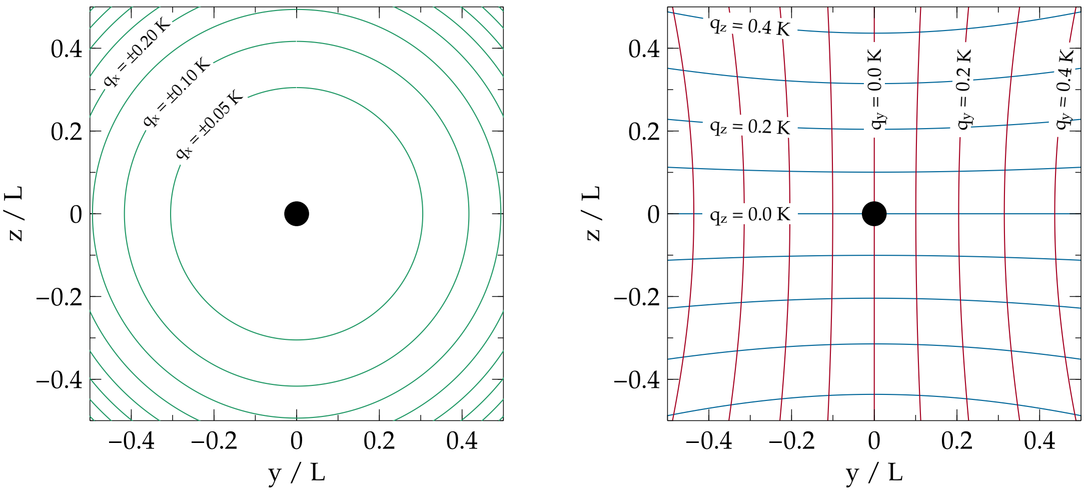

Figure 6.3: Lines of constant q_x (left), q_y or q_z (right), in units of the incident wavenumber $K = 2\pi/\lambda$, for a planar detector. SAS geometry as in Fig. 6.2.

When simulating and fitting experimental data with BornAgain, detector images remain unchanged. All work is done in terms of reduced pixel coordinates y/L and z/L. Corrections are applied to the simulated, not to the measured data.

6.1.2 Intensity transformation

The solid angle under which a detector pixel is illuminated from the sample is in linear approximation

$$\Delta\Omega = \cos\alpha_\text{f}\,\Delta\alpha_\text{f}\,\Delta\phi_\text{f} = \cos\alpha_\text{f}\left|\frac{\partial(\alpha_\text{f},\phi_\text{f})}{\partial(y,z)}\right|\Delta y\,\Delta z = \cos^3\!\alpha_\text{f}\,\cos^3\!\phi_\text{f}\,\frac{\Delta y\,\Delta z}{L^2}. \tag{6.7}$$

Altogether, the expected count rate in detector pixel (i,j) is proportional to

$$I_{ij} = \cos^3\!\alpha_\text{f}\,\cos^3\!\phi_\text{f}\,\frac{\text{d}\sigma}{\text{d}\Omega}(\mathbf{q}_{ij}), \tag{6.8}$$

where we have omitted constant factors L^{-2}, Δy and Δz. Using pixel coordinates instead of angles, this can be rewritten as

$$I_{ij} = \left(1+\frac{y^2+z^2}{L^2}\right)^{-3/2}\frac{\text{d}\sigma}{\text{d}\Omega}\big(\mathbf{q}_{ij}(y,z)\big). \tag{6.9}$$

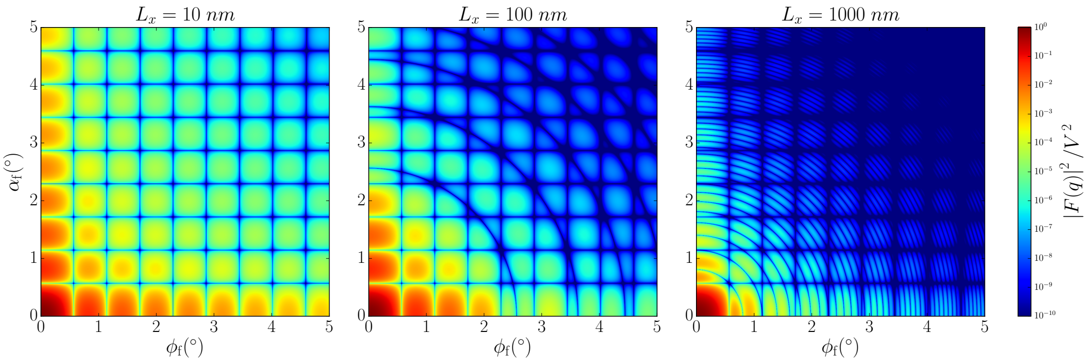

Figure 6.4: Simulated detector image for small-angle scattering from uncorrelated cuboids (right rectangular prisms). The incoming wavelength is 0.1 nm. The prisms have edge lengths $L_y = L_z = 10$ nm; the length L_x, in beam direction, is varied as shown above the plots. The circular modulation comes from a factor $\mathrm{sinc}(q_x L_x/2)$ in the cuboid form factor, with q_x given by (6.4).

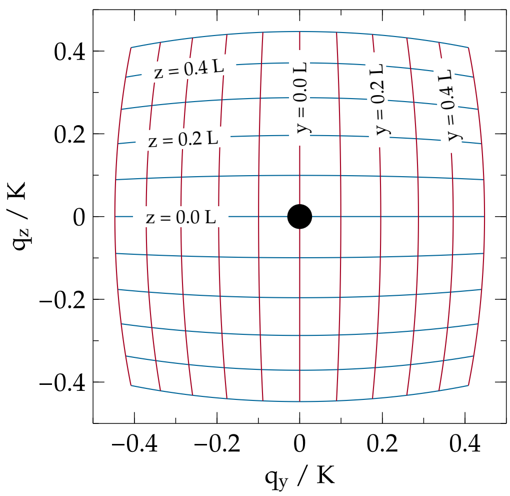

Figure 6.5: The outer contour of the blue and red grid shows the border of a square detector image after transformation into the physical coordinates q_y, q_z. The blue and red curves correspond to horizontal and vertical lines in the detector.

Bibliography

[1] G. Pospelov, W. Van Herck, J. Burle, J. M. Carmona Loaiza, C. Durniak, J. M. Fisher, M. Ganeva, D. Yurov and J. Wuttke, J. Appl. Cryst. **53**, 262 (2020). 2, 1-1, 1-4

[2] V. P. Sears, Neutron News **3**, 26 (1992). 1-2

[3] V. P. Sears, *Neutron Optics*, Oxford University Press: Oxford (1989). 1-2

[4] G. Renaud, R. Lazzari and F. Leroy, Surf. Sci. Rep. **64**, 255 (2009). 1-3

[5] M. v. Laue, Erg. exakt Naturwiss. **10**, 133 (1931). 1-3

[6] G. H. Vineyard, Phys. Rev. B **26**, 4146 (1982). 1-4

[7] P. Mazur and D. L. Mills, Phys. Rev. B **26**, 5175 (1982). 1-4

[8] S. Dietrich and H. Wagner, Z. Phys. B **56**, 207 (1984). 1-4

[9] S. Dietrich and H. Wagner, Z. Phys. B **59**, 35 (1985). 1-4

[10] H. Schober, J. Neutron Res. **17**, 109 (2014). 1-6

[11] F. Abelès, J. Phys. Radium **11**, 307 (1950). 2-6

[12] J. D. Jackson, *Classical Electrodynamics*, John Wiley: New York (^{2}1975). 2-7

[13] S. A. Stepanov, E. A. Kondrashkina, R. Köhler, D. V. Novikov, G. Materlik and S. M. Durbin, Phys. Rev. B **57**, 4829 (1998). 2-9, 2-10

[14] L. G. Parratt, Phys. Rev. **95**, 359 (1954). 2-10

[15] J. Lekner, *Theory of Reflection*, Springer: Cham (^{2}2016). 3-1, 3-2

[16] L. D. Landau and E. M. Lifschitz, *Lehrbuch der theoretischen Physik, III. Quantenmechanik*, Akademie–Verlag: Berlin (^{7}1985). 3-1, 4-2

[17] A. V. Andreev, A. G. Michette and A. Renwick, J. Mod. Opt. **35**, 1667 (1988). 3-2

[18] M. Tolan, *X-ray scattering from soft-matter thin films. Materials science and basic research* (Springer Tracts in Modern Physics 148), Springer: Berlin (1999). 3-3

[19] D. K. G. de Boer and A. J. G. Leenaers, Physica B **221**, 18 (1996). 3-3

[20] L. Névot, B. Pardo and J. Corno, Rev. Phys. Appl. **23**, 1675 (1988). 3-3

[21] A. Gibaud and G. Vignaud, in *X-ray and Neutron Reflectivity*, edited by J. Daillant and A. Gibaud (Lect. Notes Phys. 770) (2009). 3-3

[22] H. Zabel, K. Theis-Bröhl and B. P. Toperverg, in *Handbook of Magnetism and Advanced Magnetic Materials. Volume 3: Novel Techniques for Characterizing and Preparing Samples*, edited by H. Kronmüller and S. Parkin, John Wiley (2007). 4-1, 4-7

[23] M. Blume and O. C. Kistner, Phys. Rev. **171**, 417 (1968). 4-1

[24] O. Schärpf, J. Appl. Cryst. **11**, 626 (1978). 4-1

[25] E. Kentzinger, U. Rücker and B. Toperverg, Physica B **335**, 82 (2003). 4-2, 4-7

[26] E. Kentzinger, U. Rücker, B. Toperverg, F. Ott and T. Brückel, Phys. Rev. B **77**, 104435 (2008). 4-2

[27] B. P. Toperverg, in *Polarized neutron scattering*, edited by T. Brückel (Schriften des Forschungszentrums Jülich, Reihe Materie und Material 12), Forschungszentrum Jülich: Jülich (2002). 4-4, 4-6

[28] A. Rühm, B. P. Toperverg and H. Dosch, Phys. Rev. B **60**, 16073 (1999). 4-6

[29] W. G. Williams, *Polarized Neutrons*, Clarendon: Oxford (1988). 4-9

Index